Carderock Division
Naval Surface Warfare Center
9500 MacArthur Blvd.
West Bethesda, MD 20817-5700

NSWCCD-SIG-97/060-7250 March 1997

Signatures Directorate
Research and Development Report

NSWCCD-SIG-97/060-7250 Feasibility of Implementing Near-field Acoustic Holography at Large Scale

Feasibility of Implementing Near-field Acoustic Holography at Large Scale

by

Gerard P. Carroll

Approved for public release; Distribution is unlimited.

UNCLASSIFIED

SECURITY CLASSIFICATION OF THIS PAGE

REPORT DOCUMENTATION PAGE

Form Approved
OMB No. 0704-0188

1a. REPORT SECURITY CLASSIFICATION Unclassified	1b. RESTRICTIVE MARKINGS None
2a. SECURITY CLASSIFICATION AUTHORITY	3. DISTRIBUTION / AVAILABILITY OF REPORT Approved for public release. Distribution is unlimited.
2b. DECLASSIFICATION/DOWNGRADING SCHEDULE	
4. PERFORMING ORGANIZATION REPORT NUMBER(S) NSWCCD-SIG-97/060-7250	5. MONITORING ORGANIZATION REPORT NUMBER(S)
6a. NAME OF PERFORMING ORGANIZATION NSWC, Carderock Division 6b. OFFICE SYMBOL (If applicable) Code 7250	7a. NAME OF MONITORING ORGANIZATION
6c. ADDRESS (City, State, and ZIP Code) 9500 MacArthur Blvd. West Bethesda, MD 20817-5700	7b. ADDRESS (City, State, and ZIP Code)
8a. NAME OF FUNDING/SPONSORING ORGANIZATION Office of Naval Research 8b. OFFICE SYMBOL (If applicable) ONR 334	9. PROCUREMENT INSTRUMENT IDENTIFICATION NUMBER
8c. ADDRESS (City, State, and ZIP Code) 800 N. Quincy Street Arlington, VA 22217-5660	10. SOURCE OF FUNDING NUMBERS PROGRAM ELEMENT NO. / PROJECT NO. / TASK NO. / WORK UNIT ACCESSION NO.

11. TITLE (Include Security Classification)
Feasibility of Implementing Near-field Acoustic Holography at Large Scale

12. PERSONAL AUTHOR(S)
Gerard P. Carroll

13a. TYPE OF REPORT	13b. TIME COVERED	14. DATE OF REPORT (Year, Month, Day)	15. PAGE COUNT
Research & Development	FROM 960601 TO 961127	1997 March 31	46

16. SUPPLEMENTARY NOTATION

17. COSATI CODES			18. SUBJECT TERMS (Continue on reverse if necessary and identify by block number)
FIELD	GROUP	SUB-GROUP	Near-field Acoustic Holography; Intermediate Scale Measurement System; Helmholtz Integral Equation; Wavenumber Response; Hologram Plane Data

19. ABSTRACT (Continue on reverse if necessary and identify by block number)
This report presents the results of a numerical investigation into the technical feasibility of implementing near-field acoustic holography (NAH) at large scale using the Intermediate Scale Measurement System (ISMS). Results are presented using two data sets, one corresponding to numerically generated hologram plane pressures for the Whitefish model and the other to actual experimental data for the Naval Research Laboratory (NRL) C-50 model. The numerically generated hologram plane pressures are valid in the range ka < 4.0 while the C-50 data is valid up to ka < 20. The focus of the investigation is to determine whether or not large scale implementation of NAH is feasible given the magnitude of background noise levels and sensor placement inaccuracies likely to be encountered. Measured ambient noise levels for the ISMS range are used in this investigation. The effect of both random and systematic axial, circumferential and radial sensor placement errors are assessed and compared. The majority of the results are presented as wavenumber comparisons of
(Cont)

20. DISTRIBUTION / AVAILABILITY OF ABSTRACT ☒ UNCLASSIFIED/UNLIMITED ☐ SAME AS RPT. ☐ DTIC USERS	21. ABSTRACT SECURITY CLASSIFICATION Unclassified
22a. NAME OF RESPONSIBLE INDIVIDUAL Maidanik, G.	22b. TELEPHONE (Include Area Code) (301)227-1292 22c. OFFICE SYMBOL NSWCCD 7030

REPORT DOCUMENTATION PAGE (Continuation Sheet)

19. ABSTRACT (continued)

contaminated and uncontaminated surface pressure reconstructions. In general, the results are very favorable regarding the feasibility of implementing NAH at ISMS. It is shown that both background noise and sensor placement error result in high wavenumber noise and that the success of implementing NAH at large scale relies largely on the selection of low-pass wavenumber filters suitable for removing these contaminating factors while preserving the cylinder's actual wavenumber response.

Table of Contents

ABSTRACT

This report presents the results of a numerical investigation into the technical feasibility of implementing near-field acoustic holography (NAH) at large scale using the Intermediate Scale Measurement System (ISMS). Results are presented using two data sets, one corresponding to numerically generated hologram plane pressures for the Whitefish model and the other to actual experimental data for the Naval Research Laboratory (NRL) C-50 model. The numerically generated hologram plane pressures are valid in the range ka < 4.0 while the C-50 data is valid up to ka < 20. The focus of the investigation is to determine whether or not large scale implementation of NAH is feasible given the magnitude of background noise levels and sensor placement inaccuracies likely to be encountered. Measured ambient noise levels for the ISMS range are used in this investigation. The effect of both random and systematic axial, circumferential and radial sensor placement errors are assessed and compared. The majority of the results are presented as wavenumber comparisons of contaminated and uncontaminated surface pressure reconstructions. In general, the results are very favorable regarding the feasibility of implementing NAH at ISMS. It is shown that both background noise and sensor placement error result in high wavenumber noise and that the success of implementing NAH at large scale relies largely on the selection of low-pass wavenumber filters suitable for removing these contaminating factors while preserving the cylinder's actual wavenumber response.

ADMINISTRATIVE INFORMATION

This work was performed at the Carderock Division, Naval Surface Warfare Center. The project was funded by the Office of Naval Research (ONR 334) under the Structural Acoustics Project under the 6.2 Submarine Technology Program, Large Scale Holography Task. The project was administered at CD/NSWC by Mr. Glen Szilagyi.

1. INTRODUCTION

Near-field acoustic holography (NAH), first proposed by Maynard and Williams[1,2] has been validated in precisely controlled underwater laboratory conditions for small scale planar[3] and cylindrical models[4]. The method provides both surface-field and far-field information from near-field pressure measured on a hologram surface. The method has also been demonstrated for irregularly shaped structures (conformal holography)[5] as well as the measurement of energy flow energy flow in structures based on reconstructed pressure and velocity[6,7]. The feasibility of implementing the approach in non laboratory conditions on larger scale models has not been studied to date. The importance of doing so follows from the fact that small scale models, because of their size, often cannot include the geometric complexities necessary to accurately model the phenomena which occur at large scale. Large scale experiments on the other hand, must be conducted in large lake or ocean facilities, and therefore, not under the precisely controlled condition for which NAH has been validated. The potential error sources such as increased background noise and inexact sensor positioning which are associated with these large scale facilities, may make it not possible to implement NAH at large scale.

2. APPROACH

This paper presents an investigation into the technical feasibility of implementing NAH at large scale. The approach used in this investigation is to simulate a NAH experiment and determine the effect of background noise and sensor placement errors on the results using two different data sets. The first data set consists of analytically generated hologram plane pressures which were calculated using a SARA 2D[8] model for a periodically ribbed cylindrical shell with hemispherical end-caps (Whitefish model). The excitation corresponds to a point force located near the mid point of the cylinder. The output surface pressure and velocity was used to generate simulated hologram plane data using a Helmholtz integral formulation which utilizes a Gaussian quadrature numerical integral formulation[9]. The effect of noise was investigated by superimposing the actual background noise for the facility under consideration and then comparing the holographically reconstructed surface pressure calculated with and without added noise. The facility presently under consideration for large scale NAH is the Intermediate Scale Measurement System (ISMS) in Bayview Idaho. The effect of sensor placement errors was also investigated by using interpolation methods to calculate hologram plane pressures at locations slightly displaced from the correct measurement location (as determined from the hologram plane measurement grid). The results of this initial investigation are valid up to ka of 4.0. For higher ka values, i.e. up to ka of 20, a similar study was conducted using actual measured hologram plane pressures for the NRL C-50 model, a 1/50 scale physical model designed to be identical to Whitefish model. This experimental data set was obtained at the Naval Research Laboratories (NRL) measurement facility[10] and is considered to be relatively free of background noise and sensor placement errors. Therefore, it was possible to investigate the effect of these errors in a manner similar to that used for the simulated hologram plane data set for the Whitefish model.

3. FORMULATION

3.1 Near-field Acoustic Holography

The formulation used in this paper for cylindrical Near-field Acoustic Holography[4] is given in terms of the helical wave spectrum amplitude in Eq. (1)

$$P_n(a,k_z) = \frac{H_n(k_r a)}{H_n(k_r r_h)} P_n(r_h,k_z). \qquad (1)$$

where $P_n(a,k_z)$ and $P_n(r_h,k_z)$ are the pressure helical wave spectral amplitudes for the cylindrical surfaces r= a and $r=r_h$ corresponding to the surface of the cylinder under investigation and the hologram plane surface respectively. The terms k_z and k_r correspond to the axial and radial components respectively of the helical wave spectrum, and are related by

$$k_r = \sqrt{k^2 - k_z^2} \qquad (1a)$$

where k is the acoustic wavenumber. The expression $\frac{H_n(k_r a)}{H_n(k_r r_h)}$ corresponds to a propagator term which relates the helical wave spectra on the two surfaces to one another. The helical wave spectrum is obtained from the two dimensional Fourier transform of the spatial pressure distribution over the hologram plane $p(r_h,\phi,z)$ as indicated in Eq.(2),

$$P_n(r_h,k_z) = F_z F_\phi[p(r_h,\phi,z)] \tag{2}$$

where the Fourier transforms are defined by

$$F_z[p(\phi,z)] = \int_{-\infty}^{\infty} p(\phi,z)e^{-ik_z z}dz \tag{3a}$$

$$F_\phi[p(\phi,z)] = \frac{1}{2\pi}\int_0^{2\pi} P(\phi,z)e^{-in\phi}d\phi \tag{3b}$$

and the inverse transforms are defined by

$$F_z^{-1}[P_n(r,k_z)] = \frac{1}{2\pi}\int_{-\infty}^{\infty} P_n(r,k_z)e^{ik_z z}dk_z \tag{4a}$$

$$F_\phi^{-1}[P_n(r,k_z)] = \sum_{-\infty}^{\infty} P_n(r,k_z)e^{in\phi} \tag{4b}$$

The final result which relates the hologram plane pressure distribution to the reconstructed pressure on the cylindrical test structure is given by

$$p(a,\phi,z) = F_z^{-1}F_\phi^{-1}\left\{\frac{H_n(k_r a)}{H_n(k_r r_h)}F_z F\phi\left[p(r_h,\phi,z)\right]\right\} . \tag{5}$$

A similar formulation for reconstructing the surface velocity $v(a,\phi,z)$ from the hologram plane pressure is given as

$$v(a,\phi,z) = F_z^{-1}F_\phi^{-1}\left\{\frac{-ik_r H'_n(k_r a)}{\rho_0 ck H_n(k_r r_h)}F_z F\phi\left[p(r_h,\phi,z)\right]\right\} . \tag{6}$$

where ρ_0 is the fluid density, c is the speed of sound and k is the acoustic wavenumber.

3.2 Wavenumber Filters

In principal, Eqs. (5) and (6) are sufficient for reconstructing surface pressure and velocity from measured hologram plane pressure. However, if there is any noise or contamination in the hologram plane pressure, it will be amplified in the back propagation process. This is due to the fact that for imaginary arguments (corresponding to subsonic wave mechanisms) the term $\frac{H_n(k_r a)}{H_n(k_r r_h)}$ increases with wavenumber, so that at higher wavenumbers, where the helical wavenumber response is typically small, the noise is amplified. This problem is alleviated by wavenumber filtering the back-propagated helical wavenumber response prior to the application of the inverse Fourier transform. Typically, low-pass helical wavenumber filters with rolloff characteristics similar to those of given by Eq. (7) are used.

$$\begin{aligned} \Pi(k_r/(2k_c)) &= 1-\frac{1}{2}e^{-(1-|k_r|/k_c)/\alpha} && |k_r| < k_c \\ &= \frac{1}{2}e^{(1-|k_r|/k_c)/\alpha} && |k_r| < k_c \end{aligned} \tag{7}$$

where k_c is the filter cutoff wavenumber and α determines the filter roll-off characteristics. The cutoff wavenumber is given by

$$k_c = \sqrt{\frac{k_{z0}^2 + (n_0/a)^2}{2}} \tag{7a}$$

where k_{z0} and n_0/a are the cutoff wavenumber components along the helical wavenumber axes. Since $k_0 = n_0/a$, this corresponds to a circular low-pass wavenumber filter in helical wavenumber space. Although alternative wavenumber filtering approaches have been proposed[11], the one given by Eq. (7) is usually implemented.

3.3 Helmholtz Integral Equation

The simulated hologram plane data generated from SARA 2D estimates of the test cylinder surface pressure and velocity are obtained using the Helmholtz integral equation as given below

$$\alpha p(\mathbf{r}') = \oiint_{S_0} \left(i\rho_0 ck G(\mathbf{r}:\mathbf{r}') v_n(\mathbf{r}) - p(\mathbf{r}) \frac{\partial}{\partial n} G(\mathbf{r}:\mathbf{r}') \right) dS_0 \tag{8}$$

Equation (8) relates the pressure at a field point $p(\mathbf{r}')$ to the pressure and velocity, $p(\mathbf{r})$ and $v_n(\mathbf{r})$ on the surface of the cylinder using the free space Greens function $G(\mathbf{r}:\mathbf{r}')$ defined by

$$G(\mathbf{r}:\mathbf{r}') = \frac{e^{ikR}}{4\pi R} \tag{9}$$

where $R = |\mathbf{r} - \mathbf{r}'|$, i.e. the distance from each source point on the cylinder to each field point on the surface of the hologram plane. Hologram plane pressures were obtained from Eq. (8) using a Gaussian Quadrature formulation[9] to numerically evaluate the integrals. The integration order for the quadrature formula implemented is 2 for axial integration and 16 per wavelength in the circumferential direction.

4. PROCEDURE

4.1 Numerically Simulated Data Set

SARA estimates of the surface pressure and velocity for 996 axial points and for 16 circumferential orders were utilized in conjunction with Eq.(8) to obtain simulated hologram plane pressures at 256 axial by 128 circumferential locations. Excitation frequencies correspond to ka=2.0 to ka= 4.0 in ka=0.2 increments. Using the formulation given in Eq.(5), holographically reconstructed surface pressures were obtained. With no contaminating factors added to the hologram data set, this procedure served as a validation of the numerical implementations.

4.2 Effect of Background Noise

The effect of noise on the holographic reconstructions was investigated in the following way. Since the SARA model provides absolute response levels relative to a one pound force excitation, it is possible to determine the actual hologram plane pressure signal levels to be expected at ISMS, assuming a 50 pound shaker. Addition of actual ISMS background noise levels, shown in Fig. (1), to these hologram plane pressures and subsequent holographic reconstruction of the surface pressures from this contaminated data set reveals the effect of this contaminating influence. It was determined early in this study that background noise will not be a major factor in implementing NAH at ISMS so that placing sensors extremely close to the radiating surface will have little advantage. The results presented are for a 6 in. standoff distance which is approximately equivalent to the scale standoff distance utilized at NRL for NAH.

4.3 Effect of Sensor Placement Error

The effects of sensor placement errors was investigated by using interpolation methods to calculate hologram plane pressures at locations slightly displaced from the correct measurement location as determined from the hologram plane measurement grid. Holographically reconstructed surface pressure calculated with and without sensor placement errors were compared to determine their effect. In-plane and out-of-plane errors of the kind shown in Figs. (2) and (3) were investigated. Random sensor placement errors normally distributed about the correct sensor location and with a variance of 1 cm. were considered. Bias errors (1 cm.) of the type shown in Fig. (4) were also considered. The magnitude of the placement errors considered (1 cm.) was based upon an engineering judgment of sensor placement precision and accuracy achievable at ISMS, as well as the experience of other researchers doing experiments in similar facilities and with similar size models[12,13] .

4.4 1/50 Scale Model Data Set

Data provided by NRL for hologram plane measurements of 1/50 scale submarine model were utilized in a manner similar to the SARA simulated data to determine the effect of various contaminating influences. This model was fabricated to be an exact 1/12.5 scale of the 1/4 scale model utilized for the SARA generated simulated hologram plane data. The obvious assumption in doing this is that this experimental data is relatively free of the contaminating influences under investigation, an assumption which proved to be valid. This data set corresponds to 512 axial by 90 circumferential measurement locations. The standoff distance is .244 inches (roughly the scale equivalent of a 3 in standoff for the 1/4 scale model). For all the simulations conducted using this data, dimensions were scaled up to correspond to equivalent 1/4 scale dimensions. Details of this

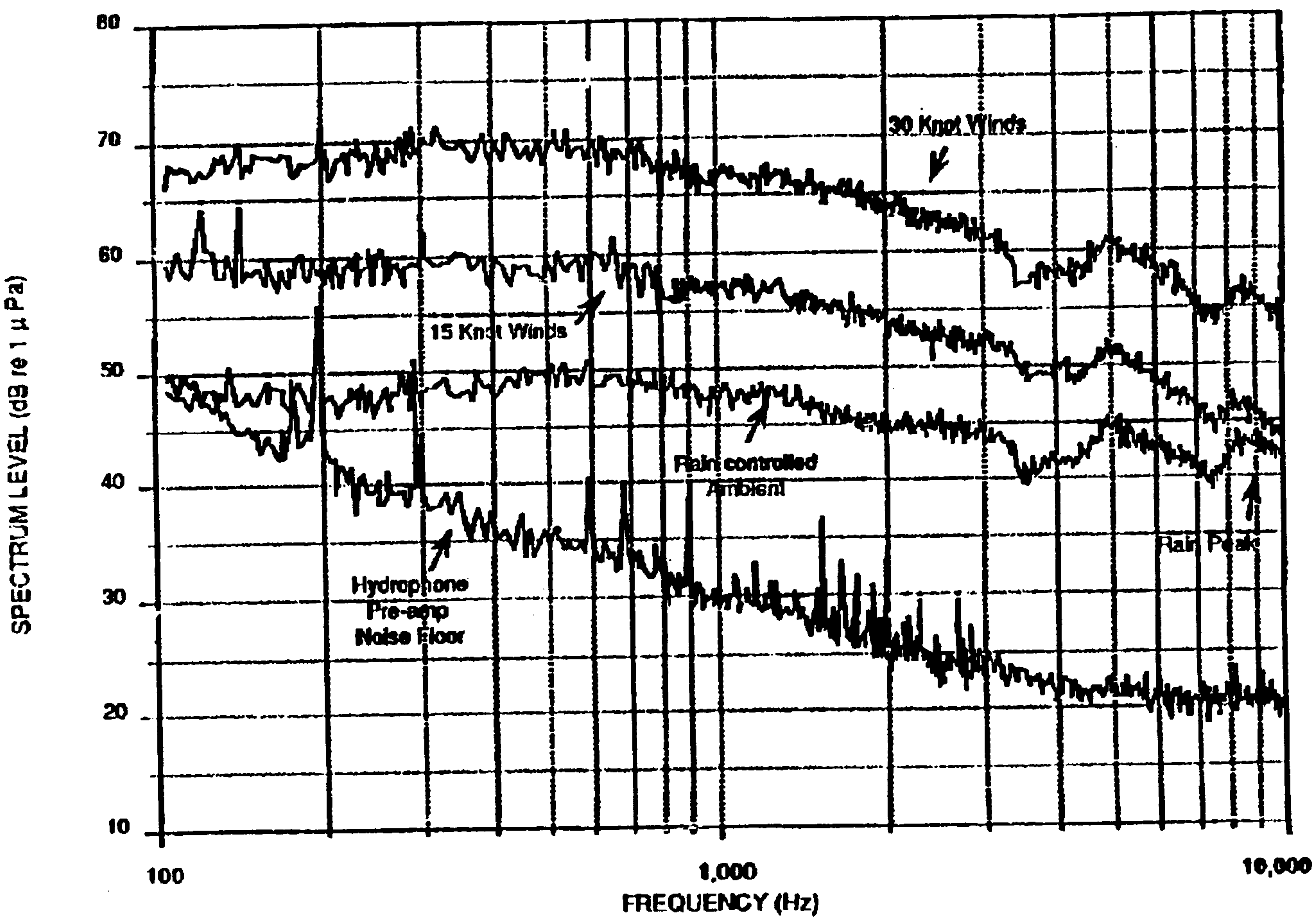

Figure 1. Sample of rain, high wind speed, and moderate wind speed controlled ambients (spectrum levels) for ISMS range.

FIG. 2(a)

AXIAL PLACEMENT RANDOM ERRORS

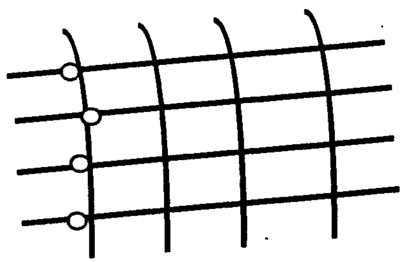

FIG. 2(b)

AXIAL & CIRCUMFERENTIAL PLACEMENT
RANDOM ERRORS

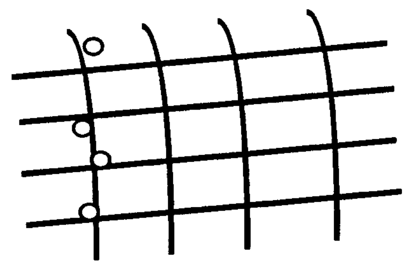

FIG. 2(c)

CIRCUMFERENTIAL PLACEMENT RANDOM ERRORS

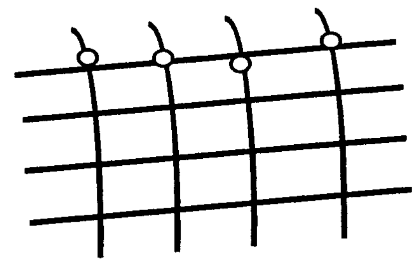

Figure 2. Random in-plane sensor placement errors considered

FIG. 3(a)

RADIAL PLACEMENT BIAS ERRORS

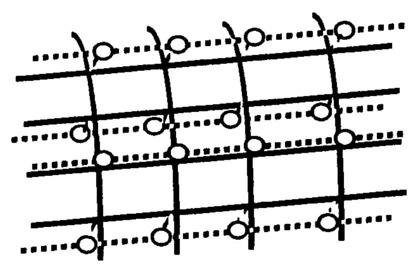

FIG. 3(b)

RADIAL OFFSET ERROR

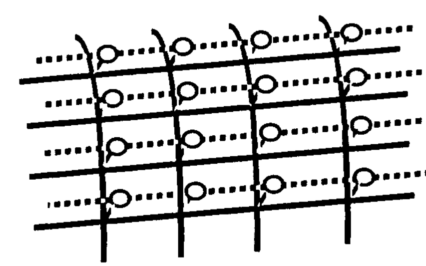

Figure 3. Random radial sensor placement errors considered

FIG. 4(a)

AXIAL PLACEMENT BIAS ERRORS

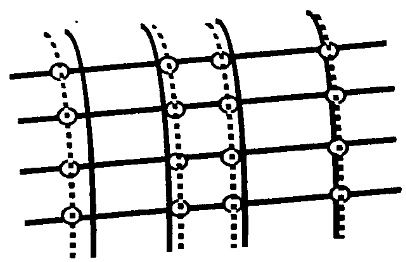

FIG. 4(b)

CIRCUMFERENTIAL BIAS ERRORS

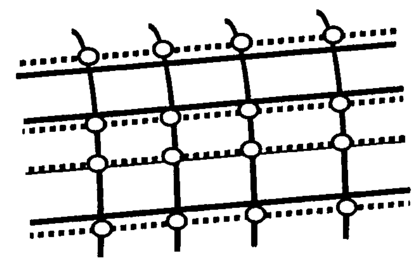

Figure 4. Sensor placement bias errors considered

model and a discussion of the physical mechanisms participating in the measured response are presented in Reference[10].

4.5 Validation of Numerical Formulations and Implementations

Figure (5) shows a cartoon depicting a graphical representation of the procedure used in this investigation. Figure 5(a) corresponds to the hologram plane pressures. For the SARA generated Whitefish data, this hologram plane data is generated using Eq. 8, and for the C-50 data, corresponds to the actual data measured at NRL. Figure 5(b) corresponds to the reconstructed surface pressures generated from the hologram plane data using the formulation given by Eq. 5 prior to the application of the inverse Fourier transform. This represents the wavenumber response of the reconstructed pressure which can be represented either as frequency versus axial wavenumber plots or as circumferential versus axial wavenumber plots as shown. Figure 5(c) shows the reconstructed surface pressure obtained by the application of the Fourier transform. A comparison of this reconstructed surface response with the SARA generated surface pressures (not shown) serves as a check of the processing algorithms. Comparisons of this type were made and indicate exact correspondence was observed.

Figures 5(d), 5(e) and 5(f) show the results obtained when the same procedure as above is applied to hologram plane data which has been modified by the various contaminating influences under investigation. The effect of these contaminating influences can then be assessed by comparing the uncontaminated and the contaminated reconstructions in either the wavenumber or the spatial domain. For the reasons given in the next section, these comparisons will be made in the wavenumber domain in this report.

4.6 The Use of Wavenumber Response

For the general example shown in Fig. 5, the effect of the contaminating influence is evident in the comparison of contaminated and uncontaminated wavenumber response. (The radiation circle is shown in the figure as a reference.) The effect of data contamination is evident as high wavenumber "noise" which occurs at a sufficiently high wavenumber so that it can be removed by applying a low-pass wavenumber filter to the data. Comparing Fig. 5(c) with Fig. 5(f) shows that the spatial domain reconstructed surface pressure for the contaminated data is identical to the

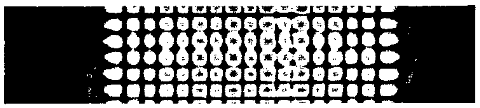

FIG. 5a. Uncontaminated hologram plane pressure

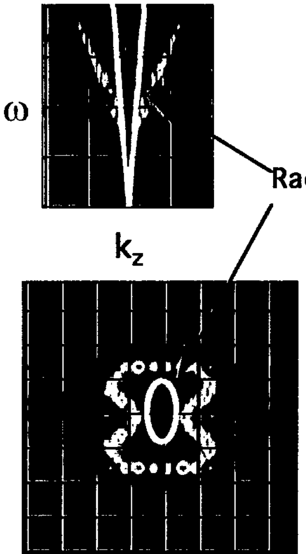

FIG. 5b. Uncontaminated Surface Pressure Reconstruction (Wavenumber Domain)

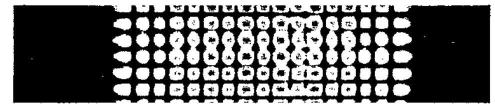

FIG 5c. Uncontaminated Surface Pressure Reconstruction (Spatial Domain)

FIG. 5d. Contaminated hologram plane pressure

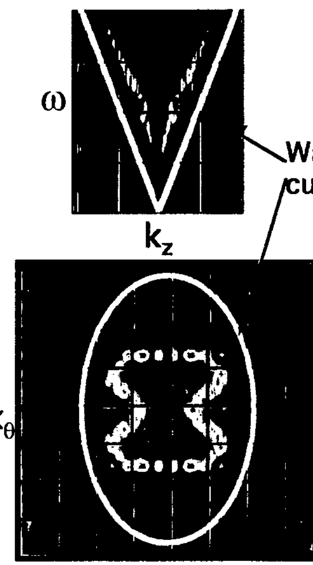

FIG. 5e. Contaminated Surface Pressure Reconstruction (Wavenumber Domain)

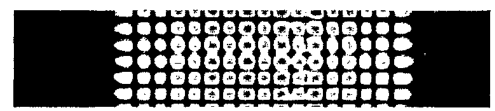

FIG. 5f. Contaminated Surface Pressure Reconstruction (Spatial Domain)

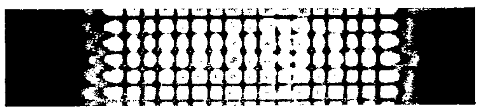

FIG. 5a. Uncontaminated hologram plane pressure

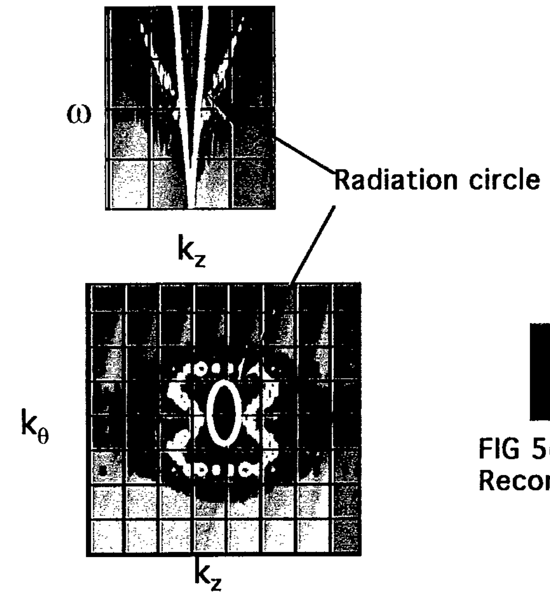

FIG. 5b. Uncontaminated Surface Pressure Reconstruction (Wavenumber Domain)

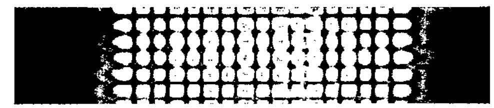

FIG 5c. Uncontaminated Surface Pressure Reconstruction (Spatial Domain)

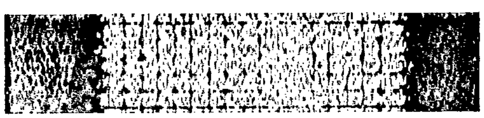

FIG. 5d. Contaminated hologram plane pressure

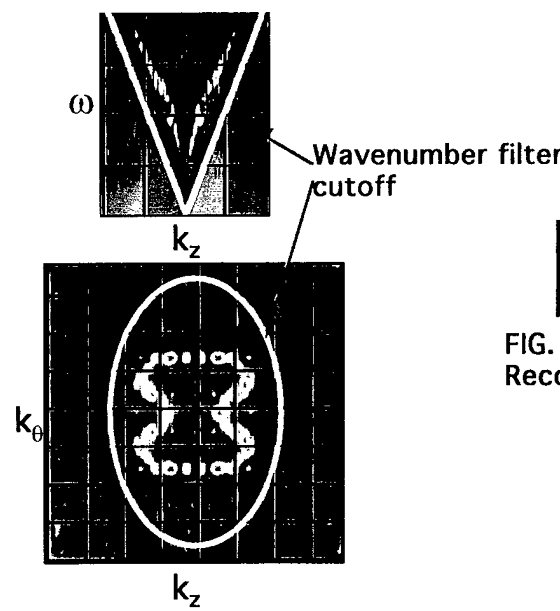

FIG. 5e. Contaminated Surface Pressure Reconstruction (Wavenumber Domain)

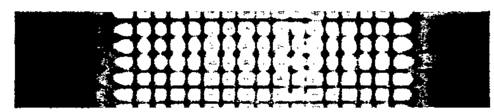

FIG. 5f. Contaminated Surface Pressure Reconstruction (Spatial Domain)

uncontaminated case after application of the wavenumber filter. Whereas Fig. 5 represents a general example, this result is representative of all the cases considered. Therefore it can be concluded that, if a low-pass wavenumber filter can be applied to contaminated data so that it eliminates the "noise" without significantly modifying the "signal", then that contaminating influence will not have an overall detrimental effect on the holographic reconstructions. In other words, if the two can be separated in wavenumber space, then holographic reconstructions are feasible. It should be pointed out that in this investigation, the use of simulated data (free from any experimental contaminating influences) makes it possible to determine what is noise and what is signal. This is not always the case in NAH experiments where contaminating influences are present. Usually the practitioner must determine, based on experience and a knowledge of the phenomena participating in the overall response, what part of the data to keep and what part to filter out.

Fig. 5 shows that typically the appropriate wavenumber filter cutoff frequency will increase with frequency. One possible approach for studying the effect of each of the contaminating influences considered is to determine what the appropriate cutoff wavenumber is for each frequency, and then to use that information to reconstruct spatial surface responses for each frequency. Such an approach would require considerable effort in determining the filter cutoff wavenumber; would result in comparisons of many reconstructed surface field pressures; and would add a subjective element to the study since the results would rely on the investigator's ability to choose the appropriate filter cutoff. A more advantageous approach is to compare the contaminated and uncontaminated wavenumber response. In this way, using a relatively small number of plots, it is possible to compare the contaminated versus uncontaminated response and determine if it would be possible to filter out the noise without greatly modifying the signal. This is the approach which will be employed in the remainder of this paper.

5. RESULTS

5.1 Hologram Plane Data Set Generated from SARA Model

Fig. 6 shows uncontaminated helical wavenumber response (circumferential versus axial wavenumber) for selected values of ka. These curves reveal many structural acoustics mechanisms associated with; wave propagation along, and radiation from, fluid loaded periodically ribbed cylinders. The mechanics revealed in the these dispersion curves however, are not the subject of this study and are discussed in detail in Reference[14] which describes a study performed on a companion cylinder to the C50 model. For the purposes of this study, the important considerations are; whether or not the features shown in the uncontaminated response curves are masked when contaminating influences are added, and; whether or not the uncontaminated response can reasonably be separated from the contaminating influences in this frequency/wavenumber domain by application of a filter.

5.1.1 Background Noise

Fig. 7. shows the reconstructed pressure helical wavenumber response when contaminated by 30 knot wind background noise. This corresponds to the highest level noise considered (see Fig. 1.). The two curves appear to be identical. This is a result of the fact that, as mentioned earlier, background noise does not appear to a major consideration for conducting NAH at ISMS. This conclusion is, however, based on the assumption of sinusoidal shaker excitation. In fact, NAH is often implemented using swept sine or chirp excitation so that, while the signal to noise will still be quite high, it may not be quite as great as that indicated. It is possible to speculate that, using shakers of this power, and since measurements are made very close to the hull for NAH experiments, the signal may be high enough to be measurable even in the presence of pleasure boating noise. If this turned out to be case, use of NAH would significantly increase the number of hours per day when acoustic measurements could be made.

5.1.2 Sensor Placement Errors

Figs. 8 through 14 show the effect of various sensor placement errors on the reconstructed helical wavenumber response. To provide a basis of comparison between the various types of

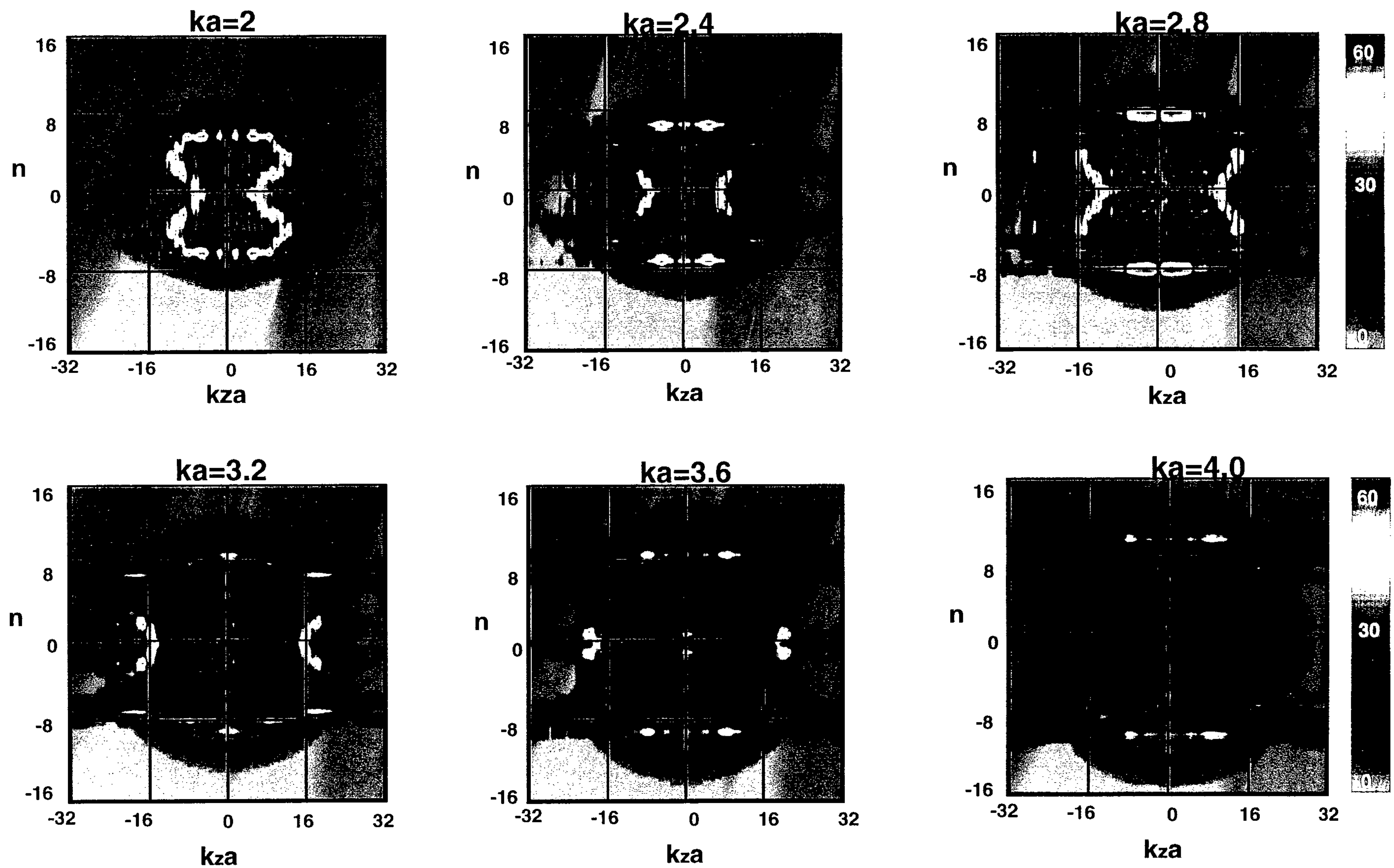

FIG. 6. Reconstructed pressure, no background noise or placement errors added

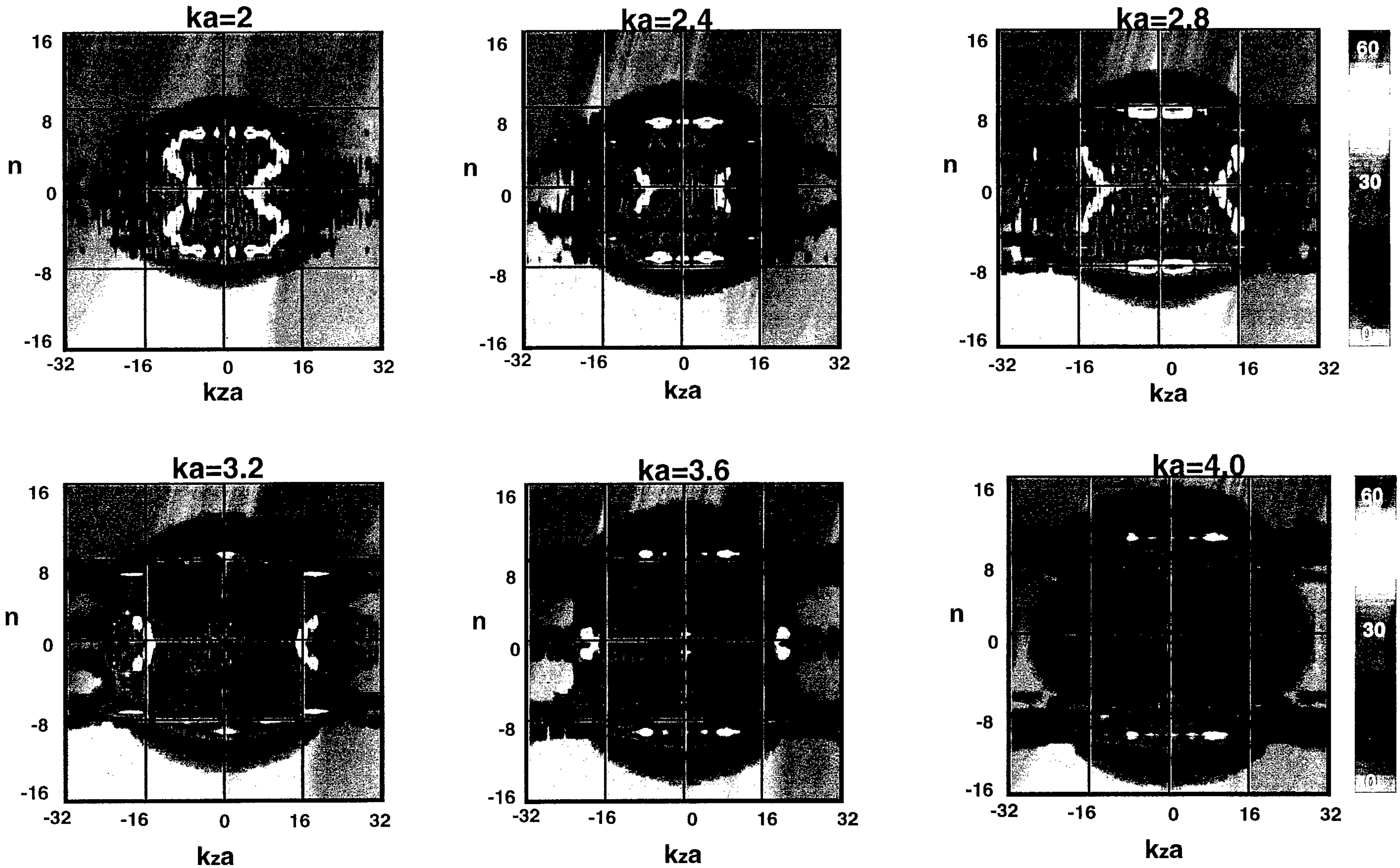

FIG. 7. Reconstructed Pressure, 30 Knot Wind Background Noise (see FIG. 1.)

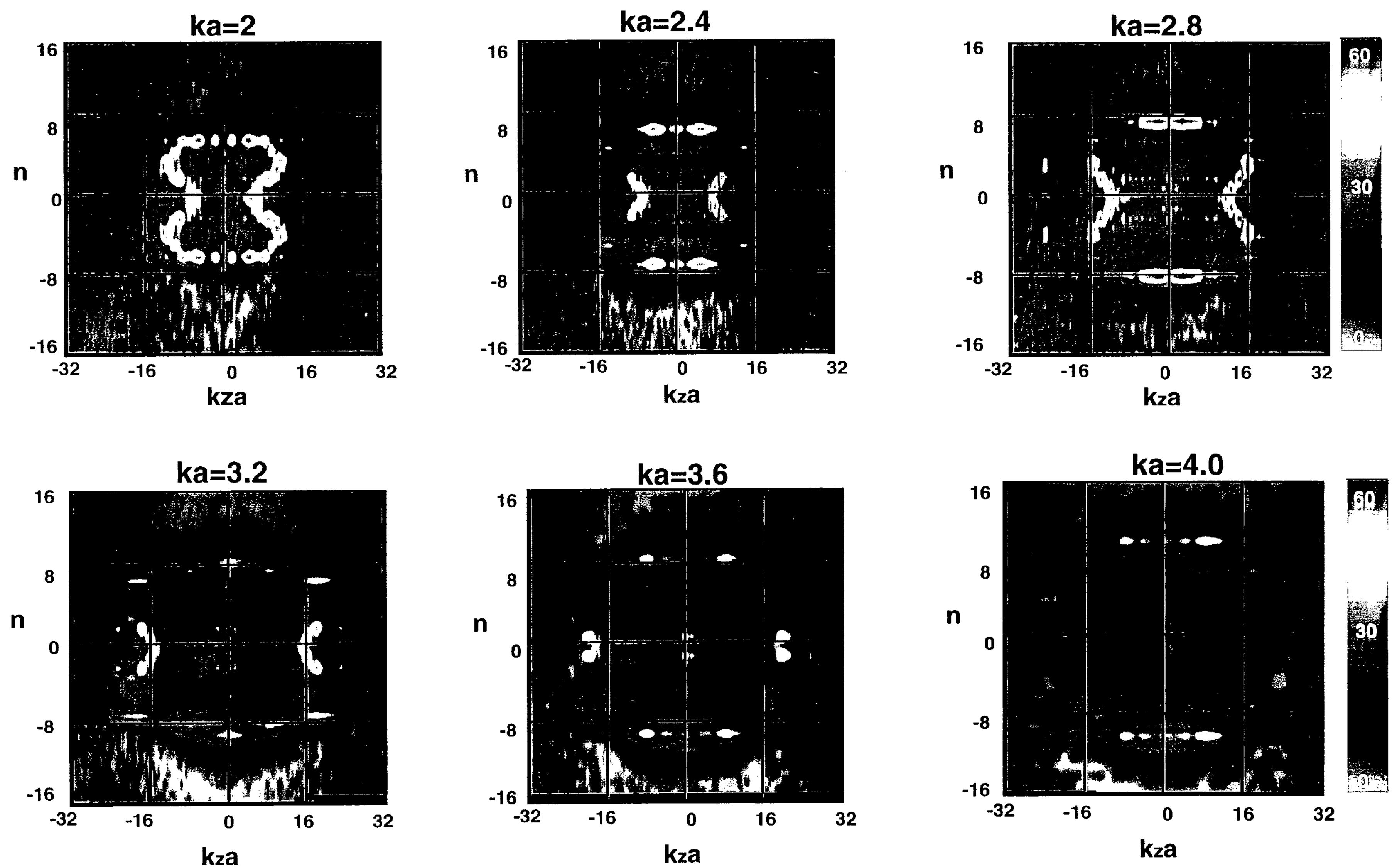

FIG. 8. Reconstructed pressure, 1cm random axial placement error (see FIG. 2(a))

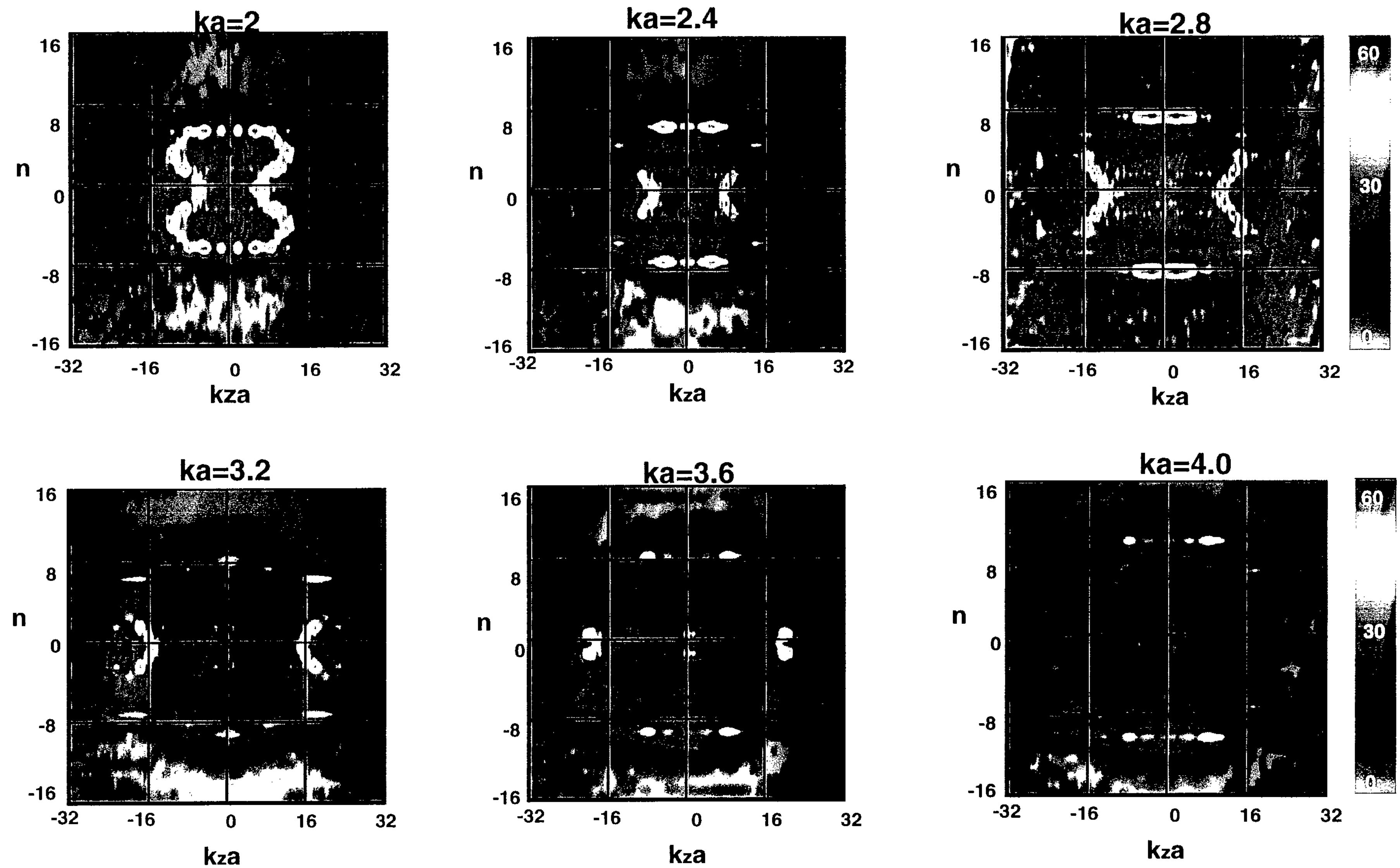

FIG. 9. Reconstructed pressure, 1cm random circumferential placement error (see FIG. 2(c))

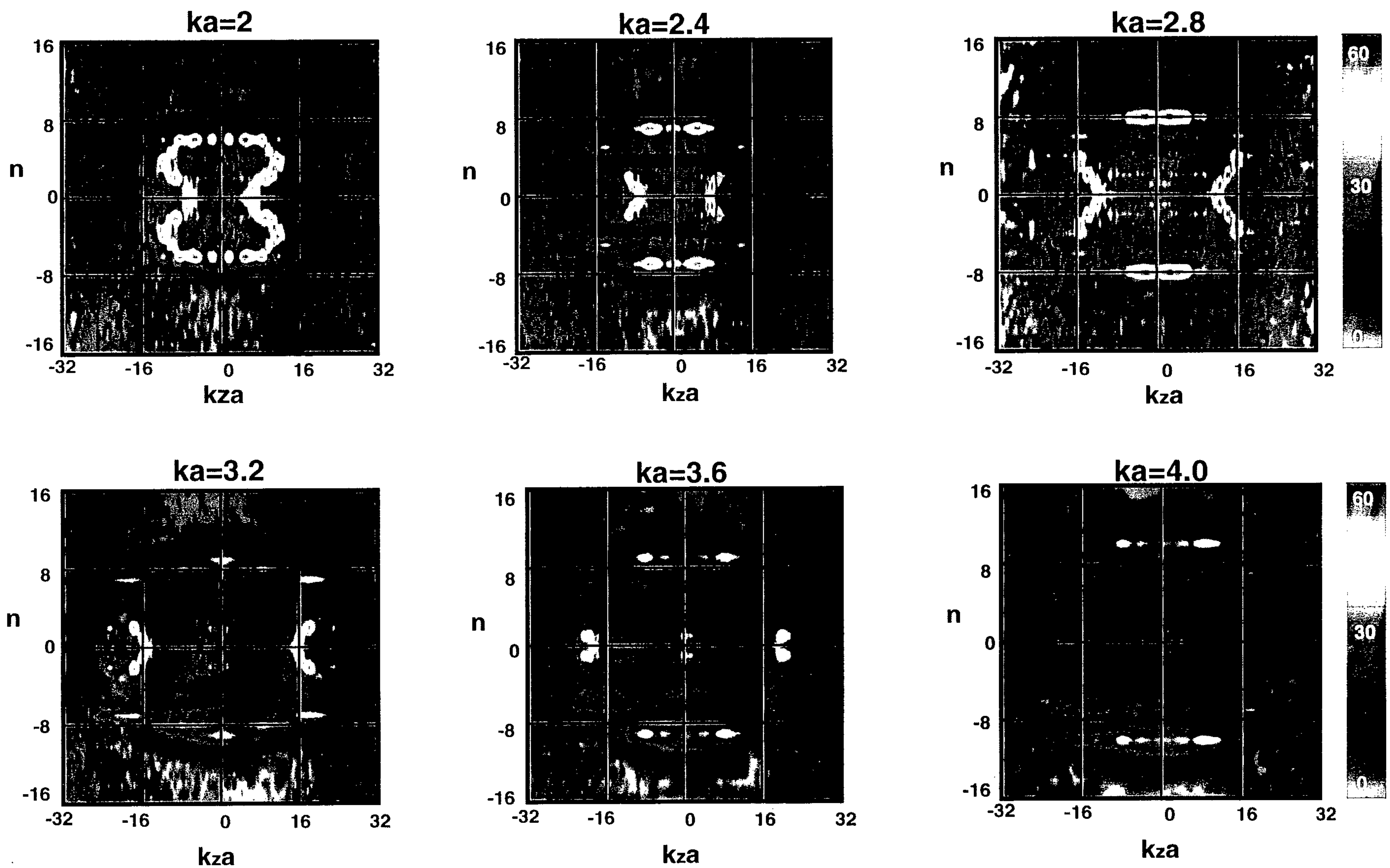

FIG. 10. Reconstructed pressure, 1cm. axial and 1cm. circumferential random placement error (see FIG. 2(c))

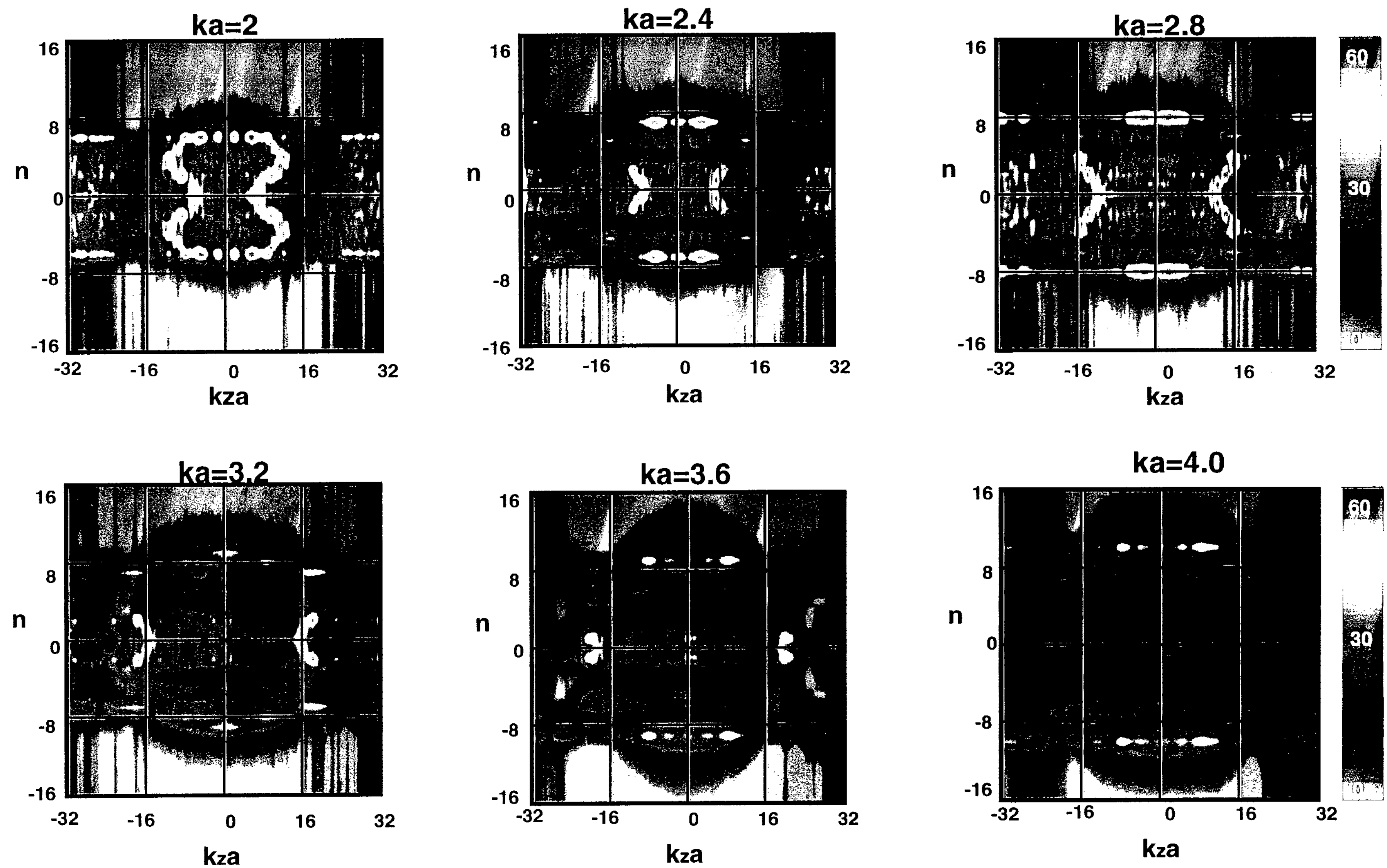

FIG. 11. Reconstructed pressure, 1cm. random axial placement error of "hoop array" (see FIG. 4(a))

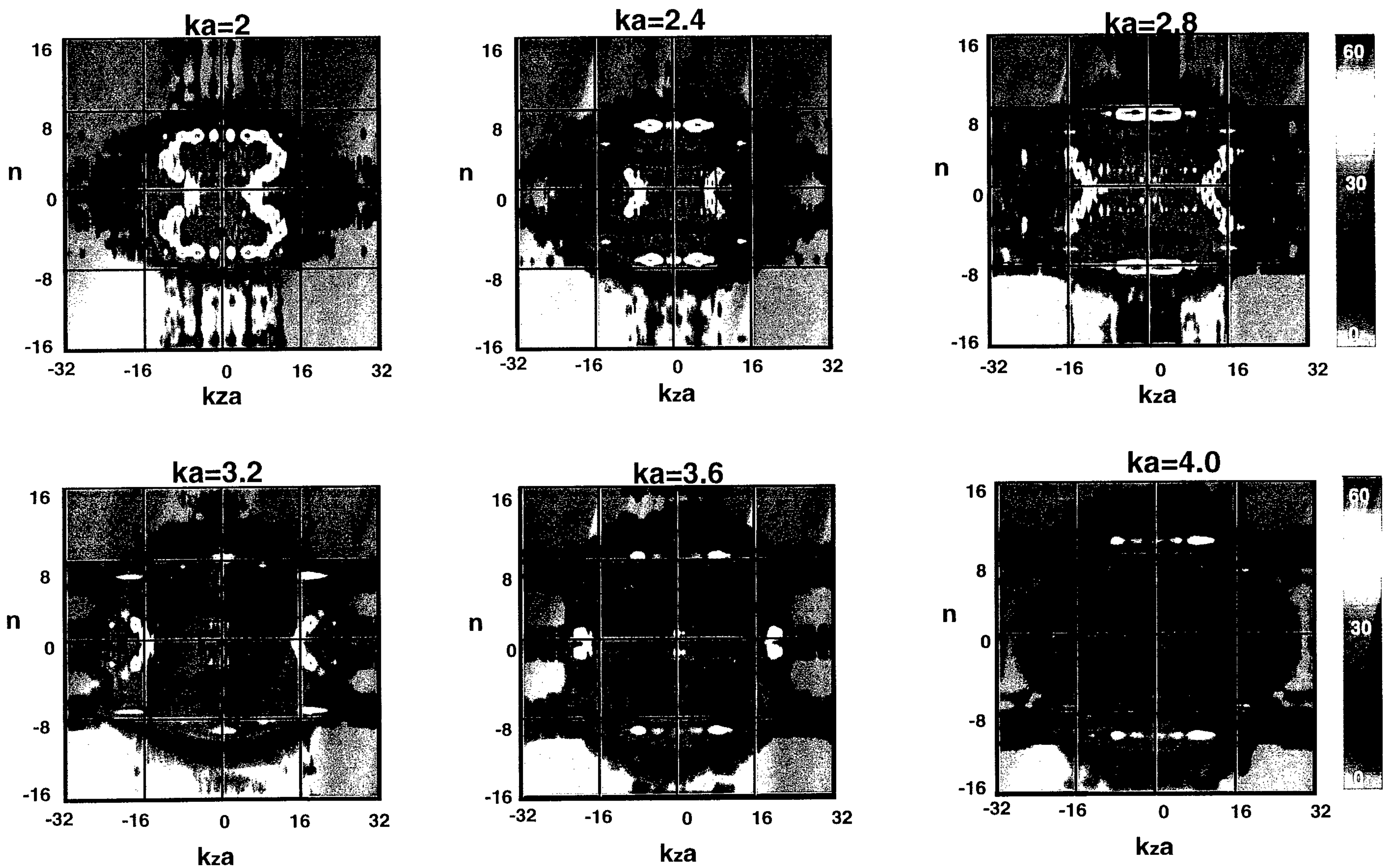

FIG. 12. Reconstructed pressure, 1cm random circumferential placement error (see FIG. 4(b))

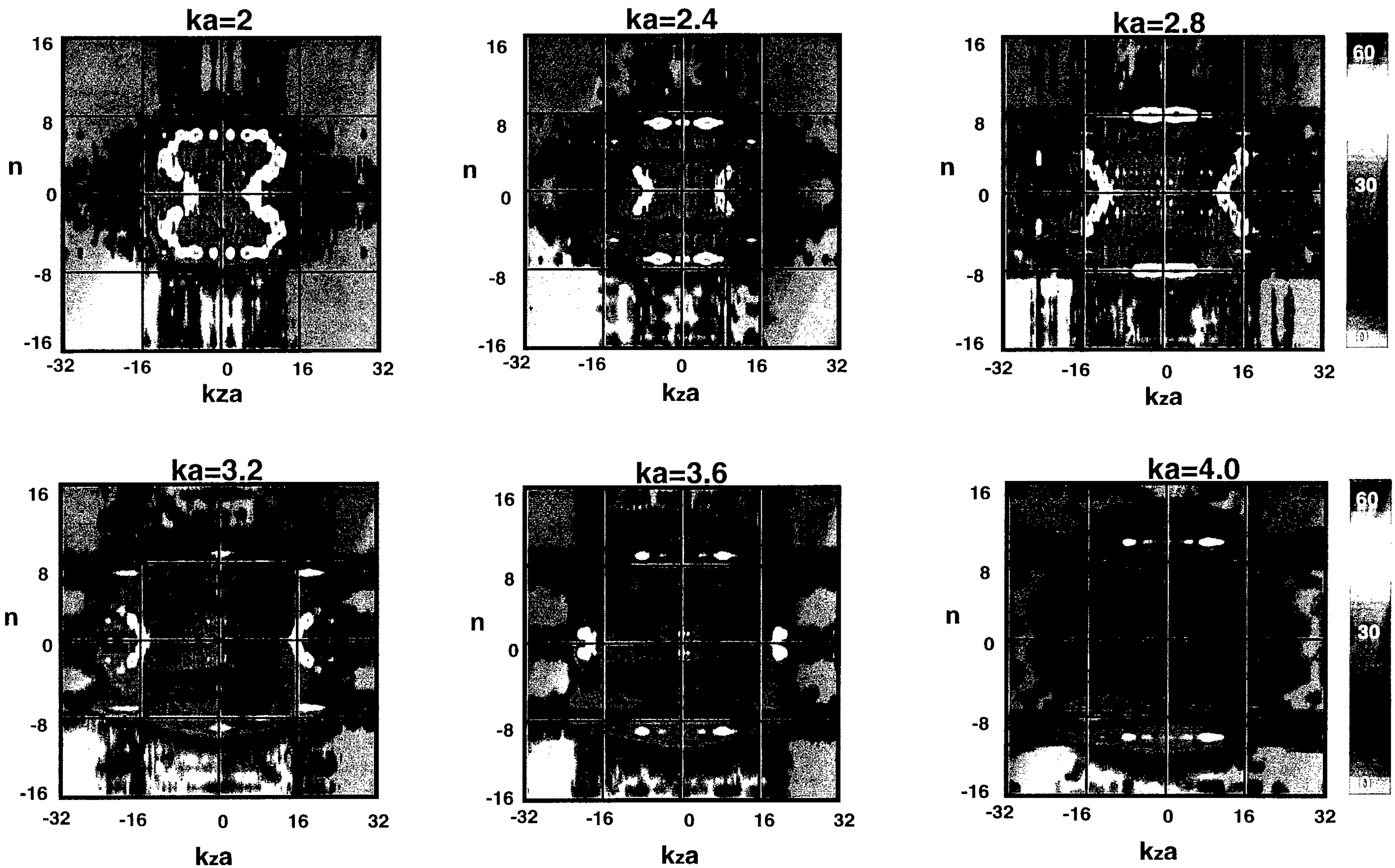

Fig 13 Reconstructed Pressure, 1cm. random radial placement error for axial line array (see Fig. 3(a))

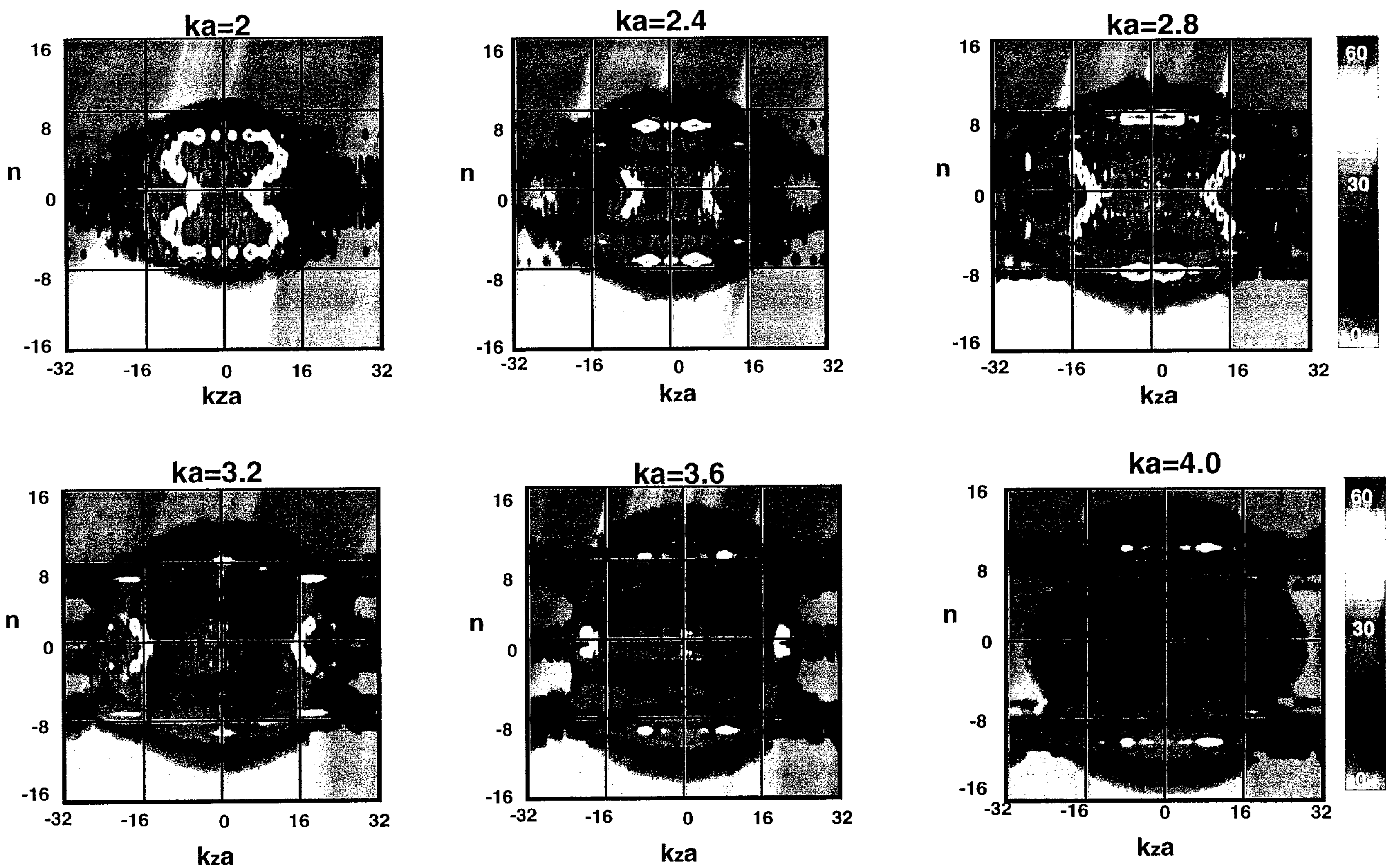

FIG. 14 Reconstructed pressure, 1cm circumferential array offset bias error (see FIG. 3(b))

placement errors considered, a placement error of 1 cm was considered for all of the data shown. For random errors this corresponds to a normally distributed random error with a variance of 1 cm about the correct placement location, and for bias errors, to a sensor placement translated 1 cm from the correct placement location. The placement errors considered can be interpreted in terms of errors associated with various methods for acquiring the hologram plane data. For example, an axial placement bias error corresponds to an axial placement error of a hoop array of hydrophones used to acquire the necessary hologram plane data by moving the array along the axis of the cylinder. Similarly, a circumferential placement bias errors corresponds to errors associated with placement of an axial array of hydrophones which acquire the necessary hologram plane data by moving the array around the circumference of the cylinder. Finally, a radial placement error could correspond to a cylindrical array of hydrophones for which longitudinal axis of the array is offset from that of the cylinder by a constant amount.

In considering the feasibility of filtering out the contaminating effects in wavenumber space, a comparison of Figs. 8 through 14 with Fig. 6 indicates that in general, for all cases shown, the important features of the helical wavenumber response are preserved when the contaminating factors are added to the data. However, at the higher wavenumbers, the wavenumber separation between the cylinder response and the contaminating factors "response" is very small at some wavenumbers. In fact, if one did not know the "true" response, (as provided by Fig. 6), it may be difficult to determine exactly where to locate the wavenumber filter cutoff frequency. Therefore, success of NAH at ISMS will require a very precise method for determining exactly where to position the cutoff. In fact, it is possible that the present practice of utilizing filters which are circular in helical wavenumber space (see Eq. 7) will not provide adequate cutoff criteria. Further research in this area is required.

This study also provides the possibility of ranking the relative contamination introduced by the various types of sensor placement errors. Such a ranking indicates that the most contamination results from random in-plane errors (axial and circumferential). Fig. 8 and 9 indicate that these error mechanisms cause roughly the same result. The next highest contamination corresponds to axial placement bias errors which have a much greater effect than circumferential placement bias errors. Circumferential placement bias errors have an effect similar to radial placement bias errors. The smallest effect is due to axial offset radial errors. This type of error corresponds to a constant translation(1 cm) of the axis of the hologram surface.

5.2 1/50 Scale Model Hologram Plane Data Set

Figs.15 to 26 show the effect of random axial and circumferential placement errors determined from the 1/50 scale model data set. Only these two types of errors were studied since the results of the SARA generated data set indicate that they had the greatest contaminating effect. Since this data set corresponds to a maximum ka of 20, substantially higher circumferential orders need to be considered in making comparisons similar to those made in the previous section. Circumferential orders up to n=44 are included in the figures.

In general, the data leads to the same conclusions as that of the SARA data set. The dispersion characteristics evident in the uncontaminated data are evident in the contaminated data, but application of a wavenumber filter to remove the contamination is possible, but may prove to be difficult. Also, as was the case with the SARA generated data set, the contamination corresponding to these two types of errors is about equivalent. The most important conclusion which can be drawn from the studies using this and the previous data set, is that, for errors of the magnitude of those considered in this study, NAH seems to be possible for ka as high as ka=20.

6. CONCLUSIONS & RECOMMENDATIONS

The following conclusions can be made on the basis of the simulations described in this paper:

1. NAH appears to be possible at ISMS if noise and placement errors do not exceed those considered in this study. It is possible that larger errors will not alter this conclusion, although such errors would need to be examined.

2. Background noise does not appear to a major consideration for conducting NAH at ISMS. In fact, especially when sinusoidal shaker excitations are considered, the signal to noise ratio may be high

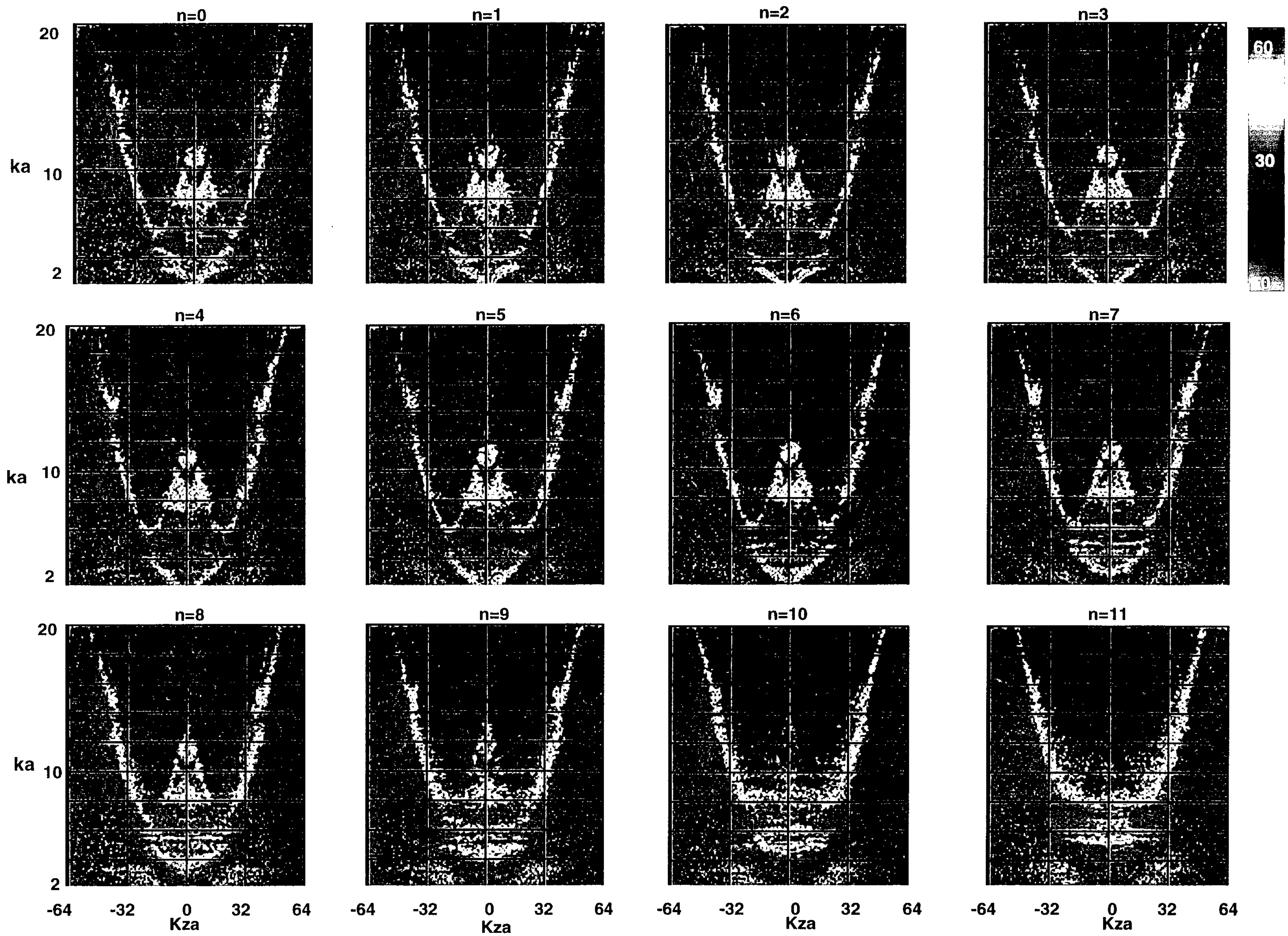

FIG. 15. Reconstructed pressure dispersion for 1/50 scale model data (n=1-11), no added contamination

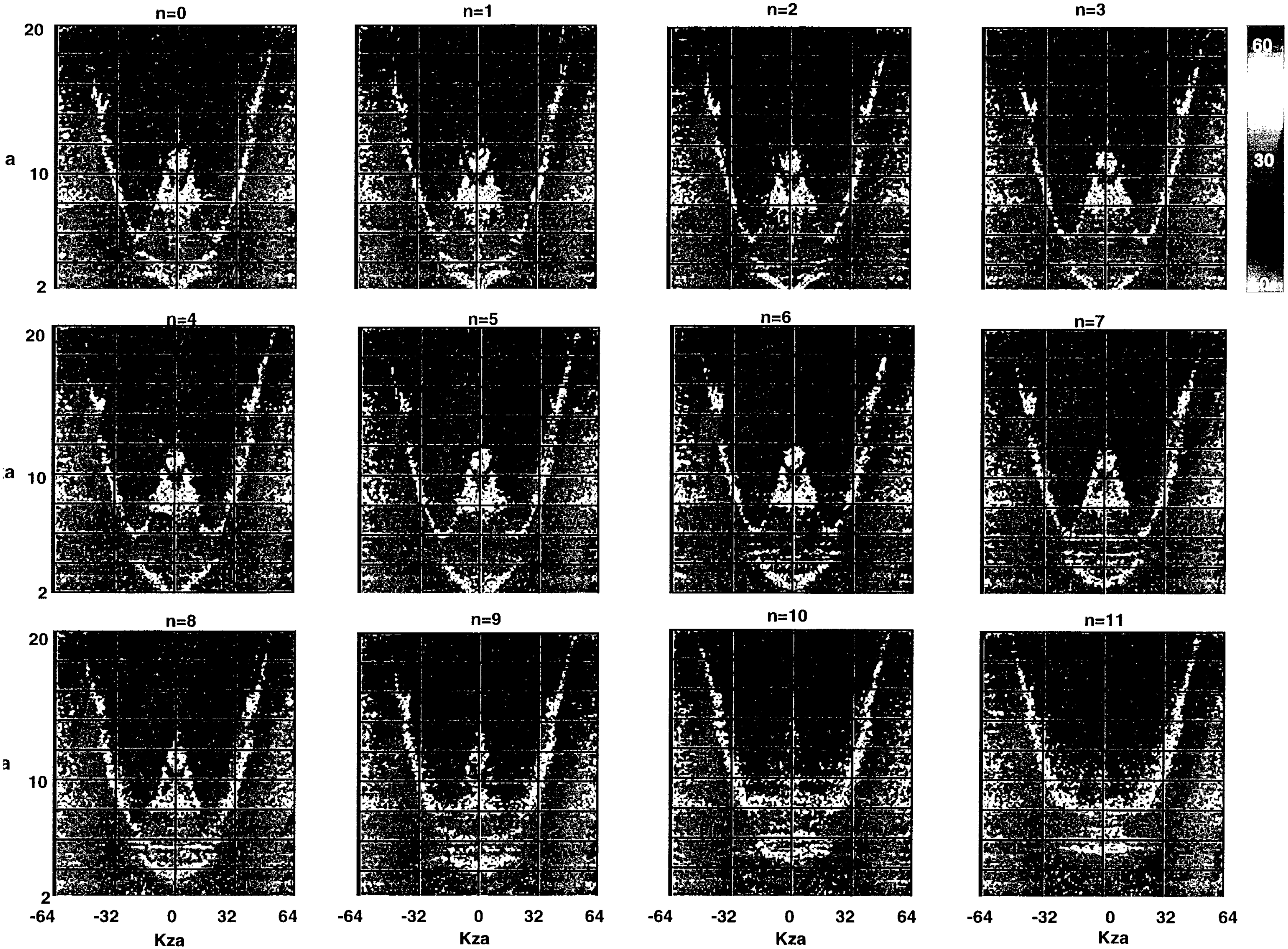

FIG. 16 Reconstructed pressure dispersion for 1/50 scale model data (n=1-11), random axial placement error

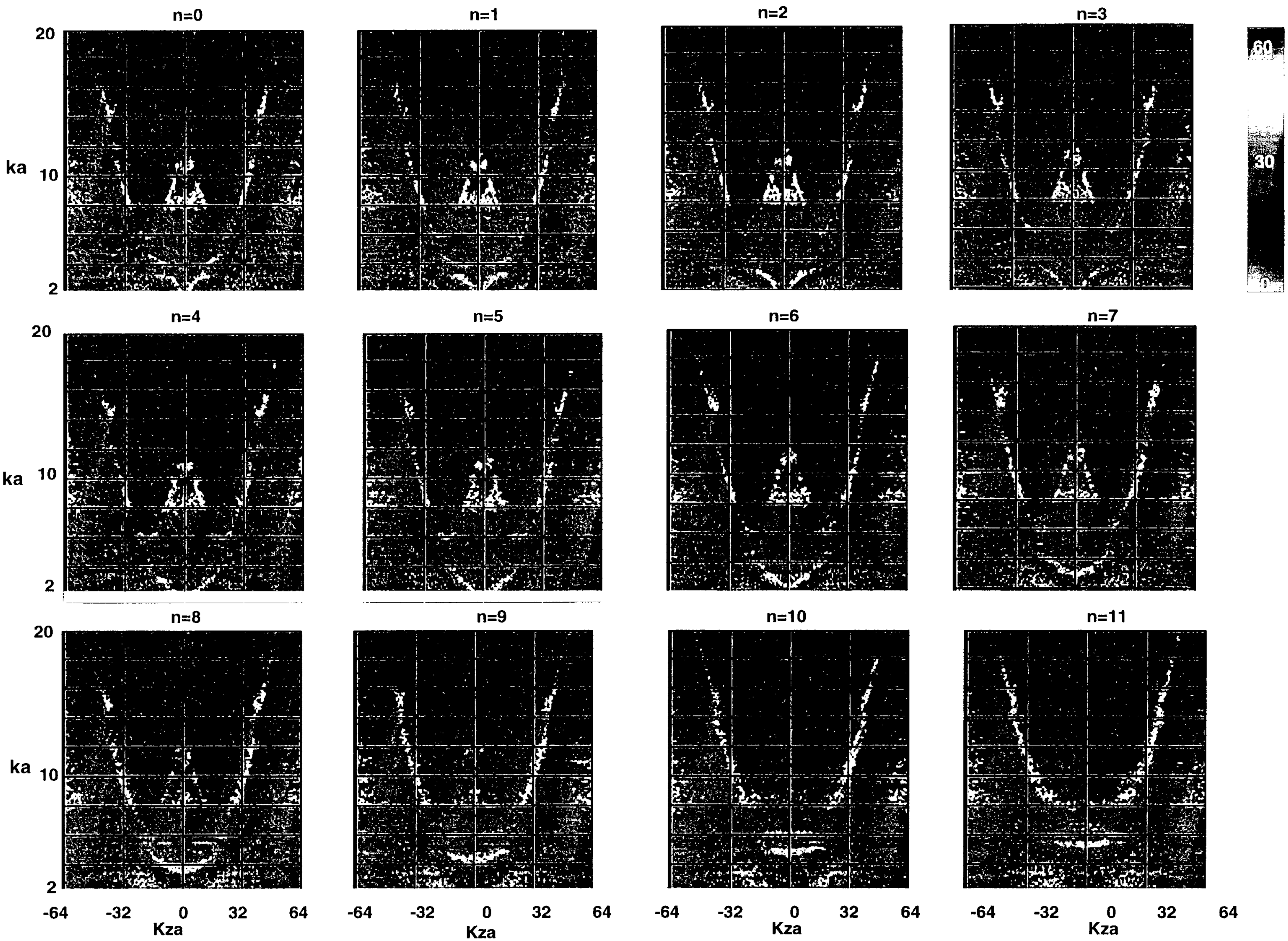

FIG. 17 Reconstructed pressure dispersion for 1/50 scale model data (n=1-11), random circumferential placement error

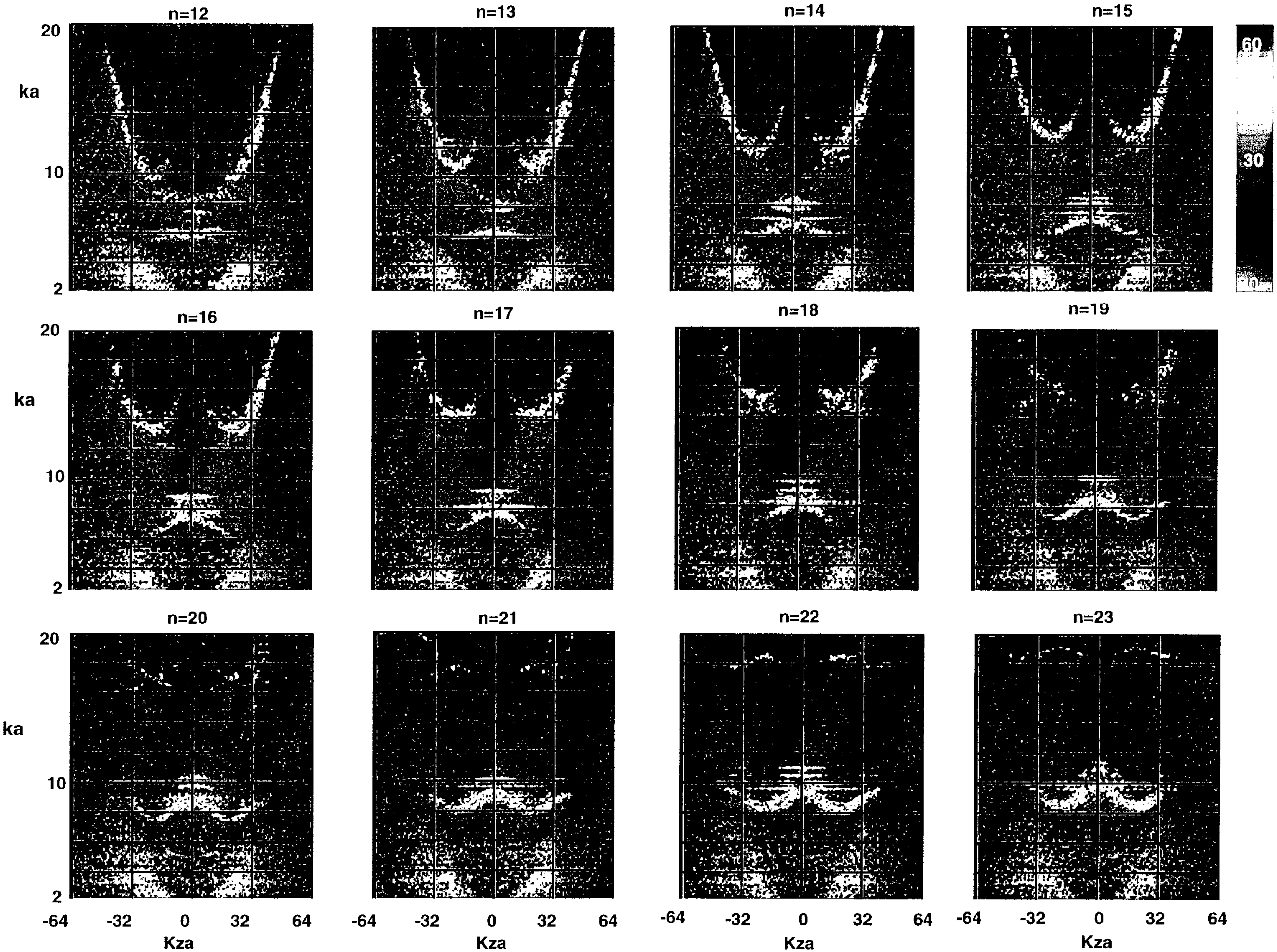

FIG. 18 Reconstructed pressure dispersion for 1/50 scale model data (n=12-23), no added contamination

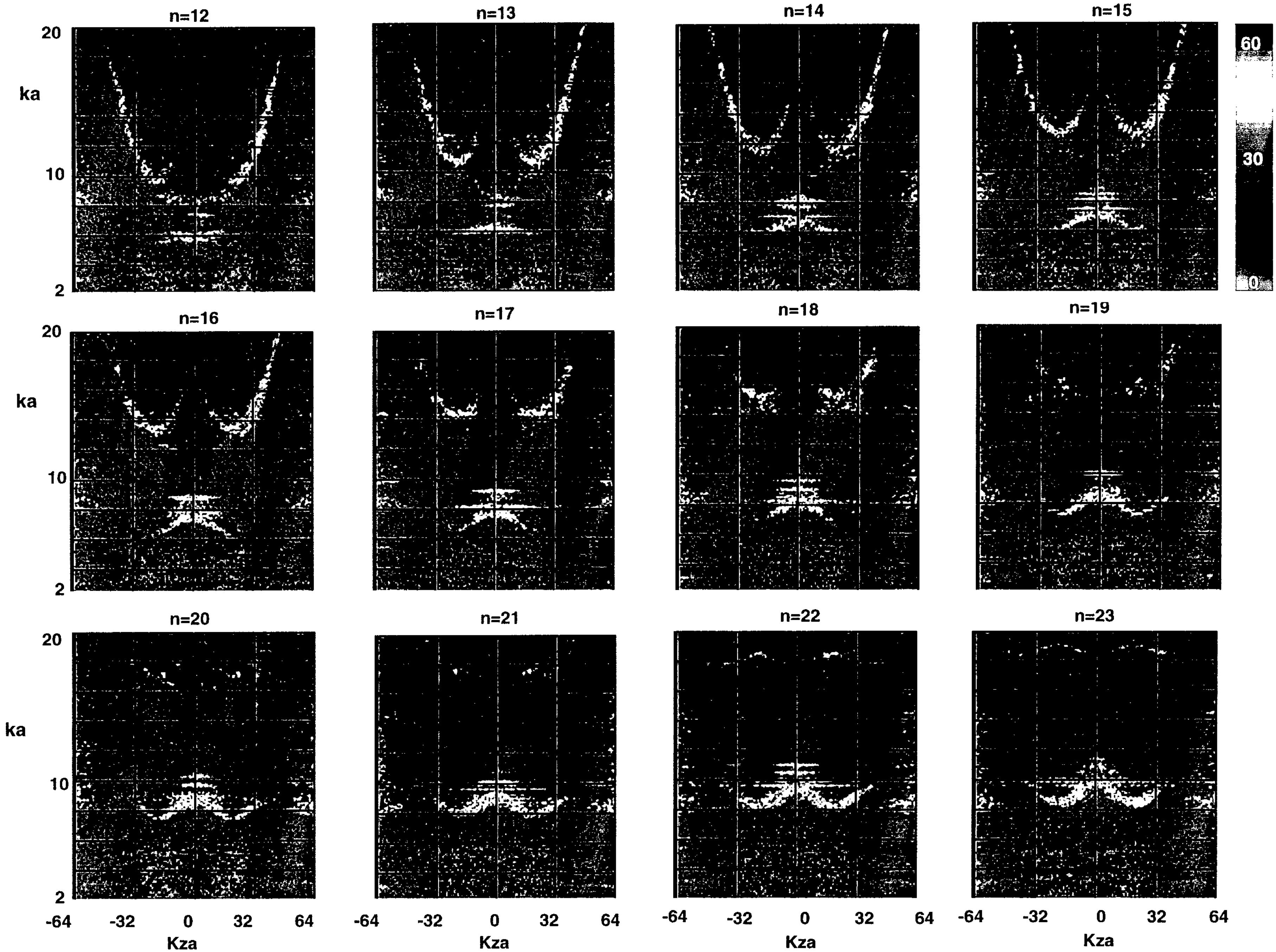

FIG. 19. Reconstructed pressure dispersion for 1/50 scale model data (n=12-23), random axial placement error

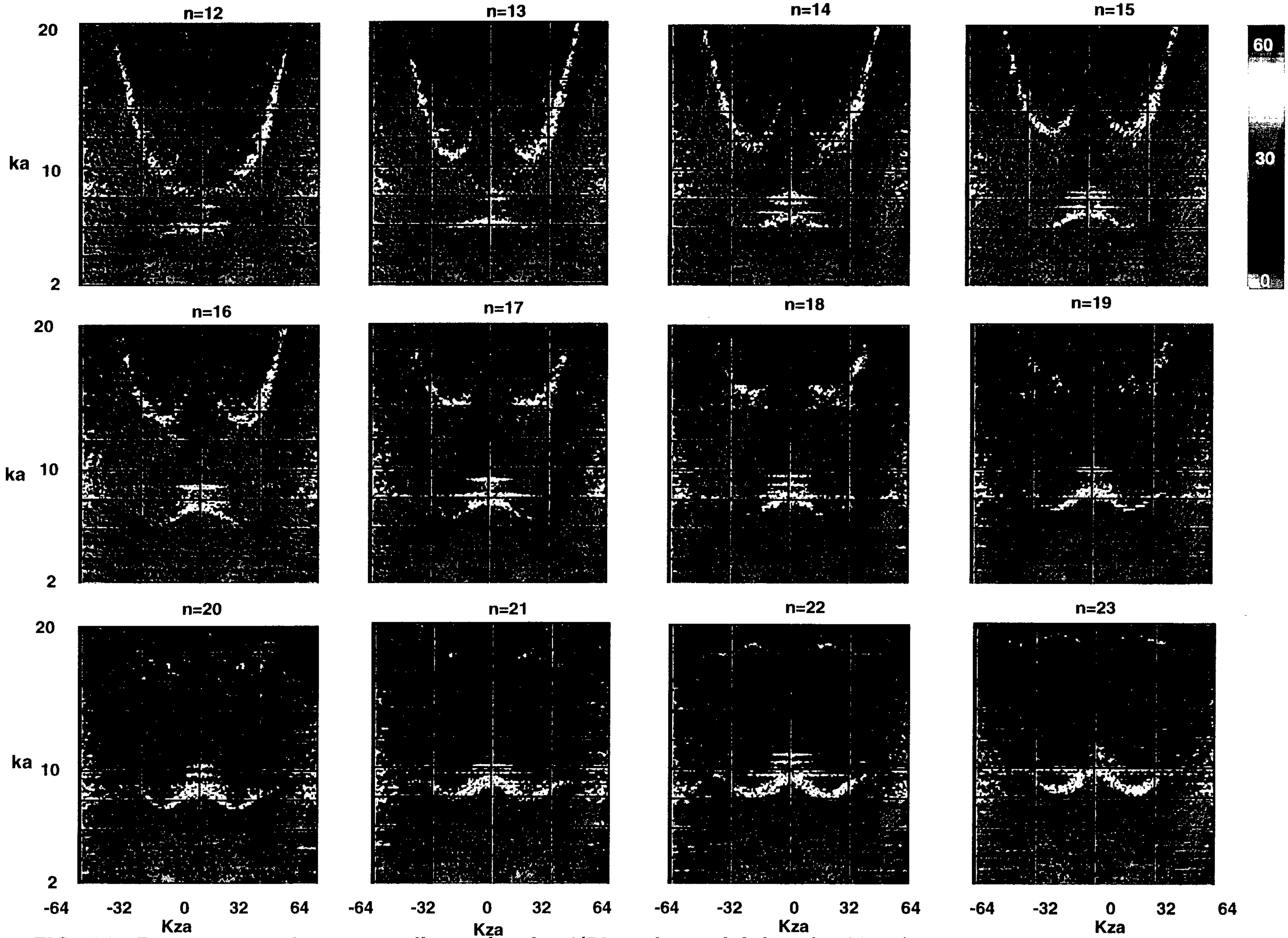

FIG. 20. Reconstructed pressure dispersion for 1/50 scale model data (n=12-23), random circumferential placement error

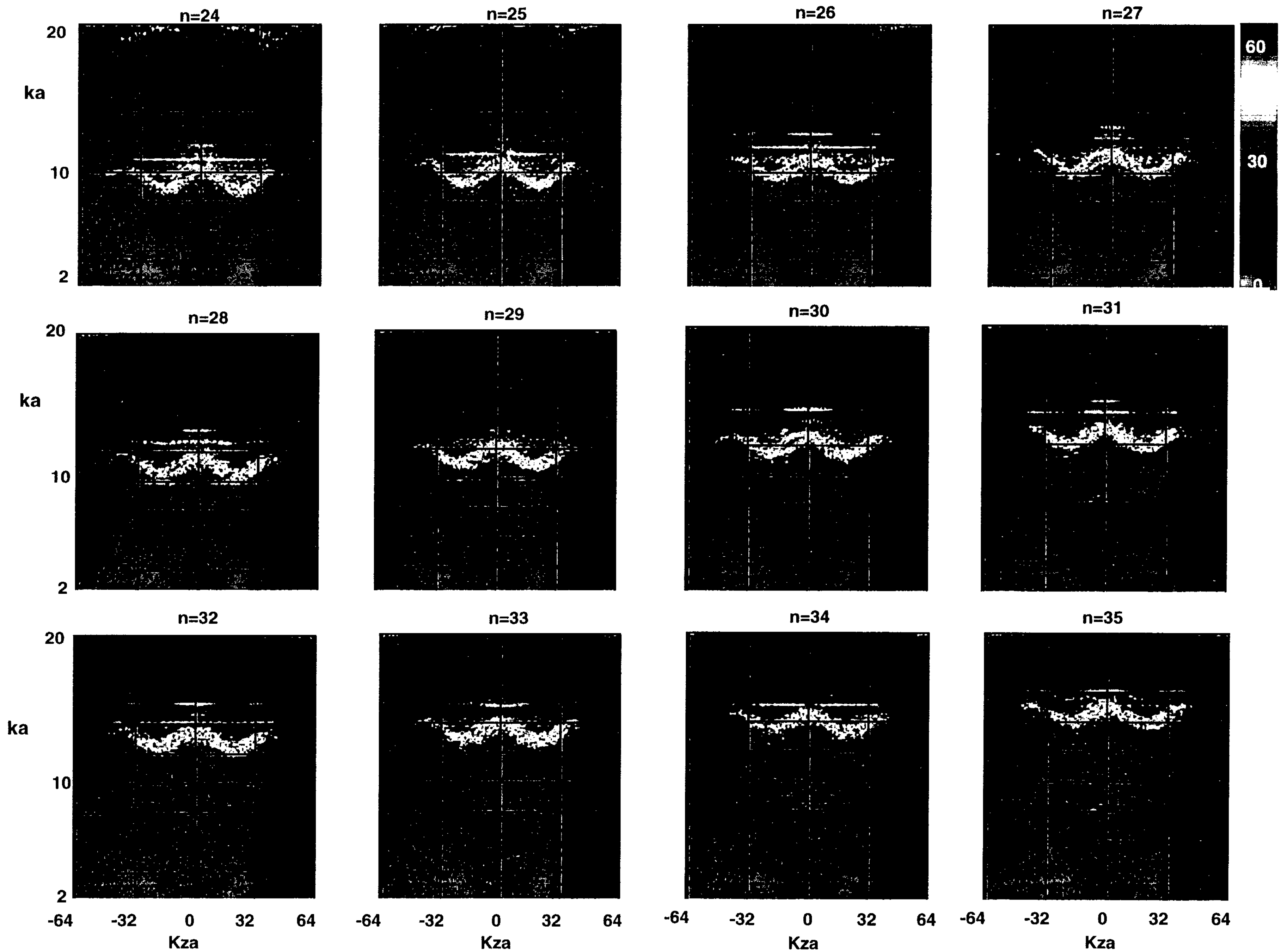

FIG. 21. Reconstructed pressure dispersion for 1/50 scale model data (n=24-35), no added contamination

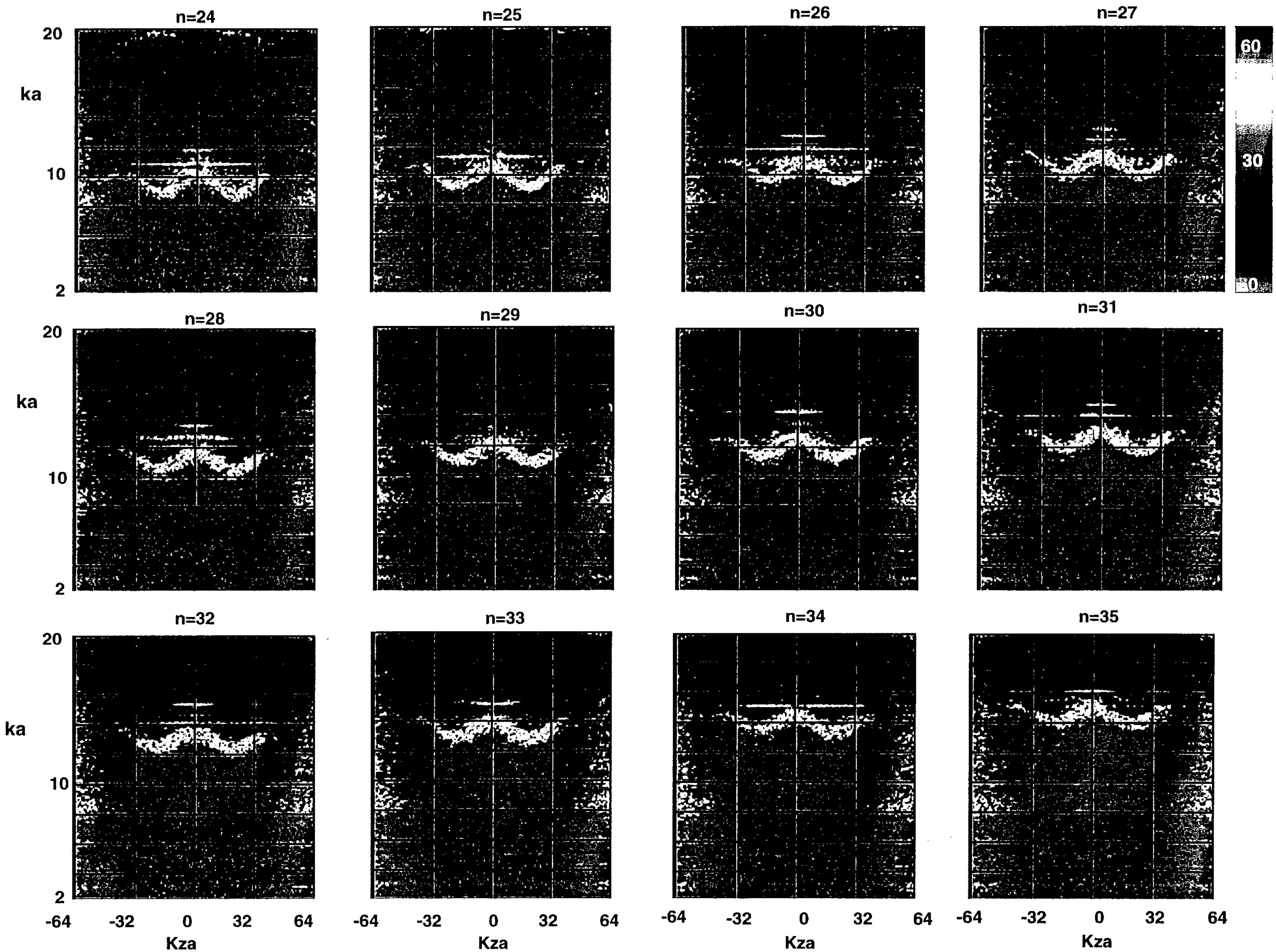

FIG. 22. Reconstructed pressure dispersion for 1/50 scale model data (n=24-35), random axial placement error

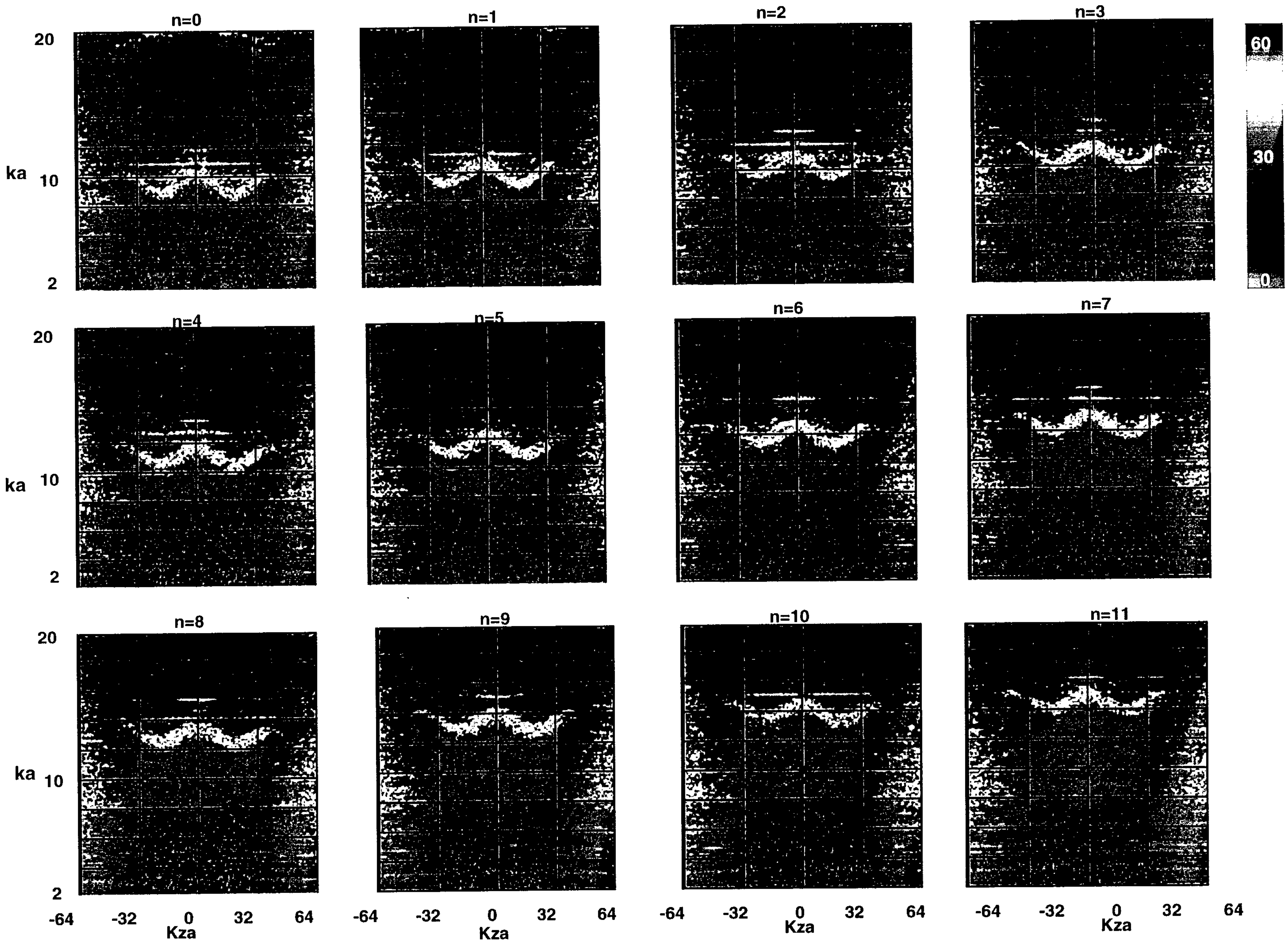

FIG. 23. Reconstructed pressure dispersion for 1/50 scale model data (n=24-35), random circumferential placement error

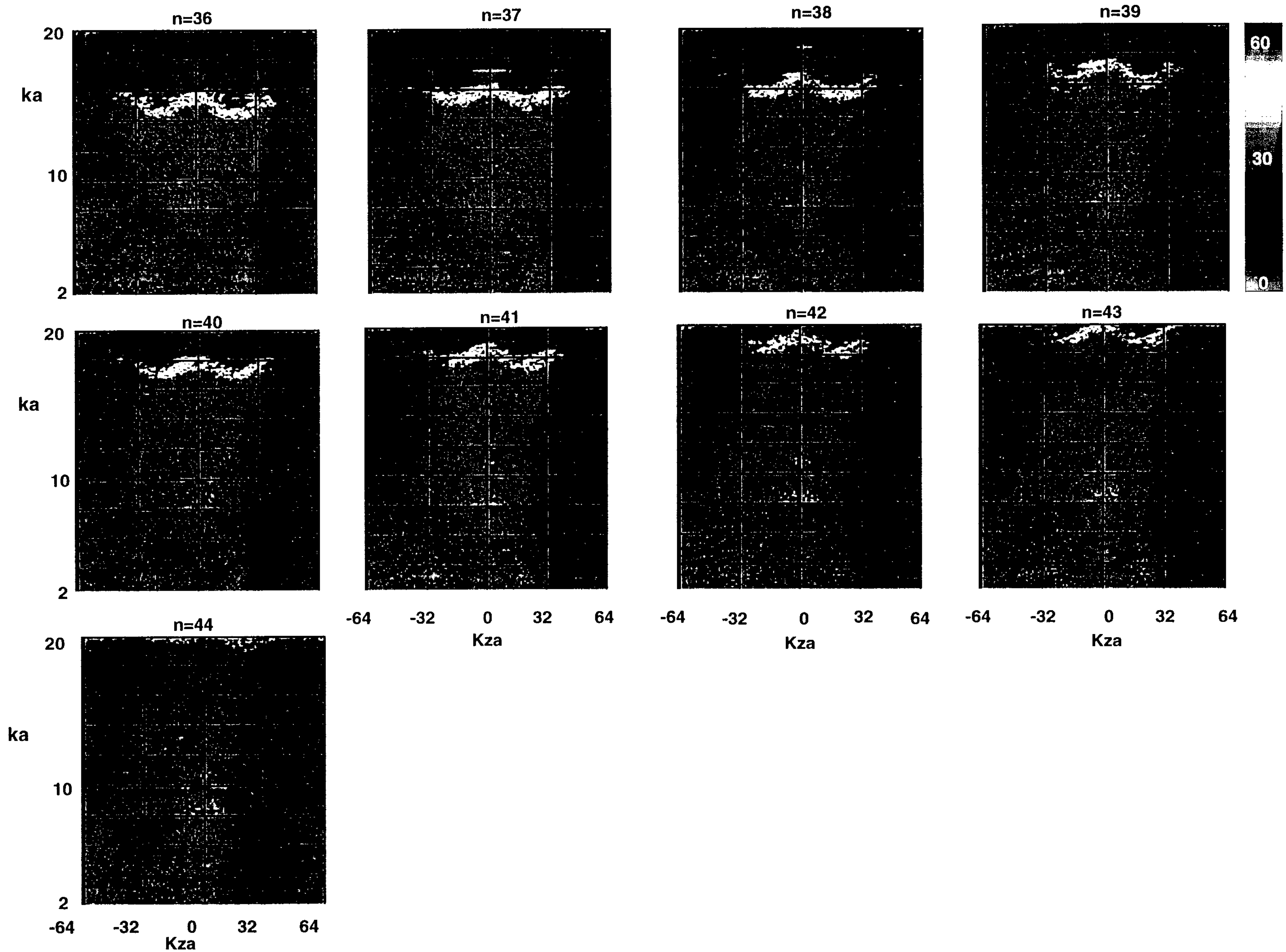

FIG. 24. Reconstructed pressure dispersion for 1/50 scale model data (n=36-44), no added contamination

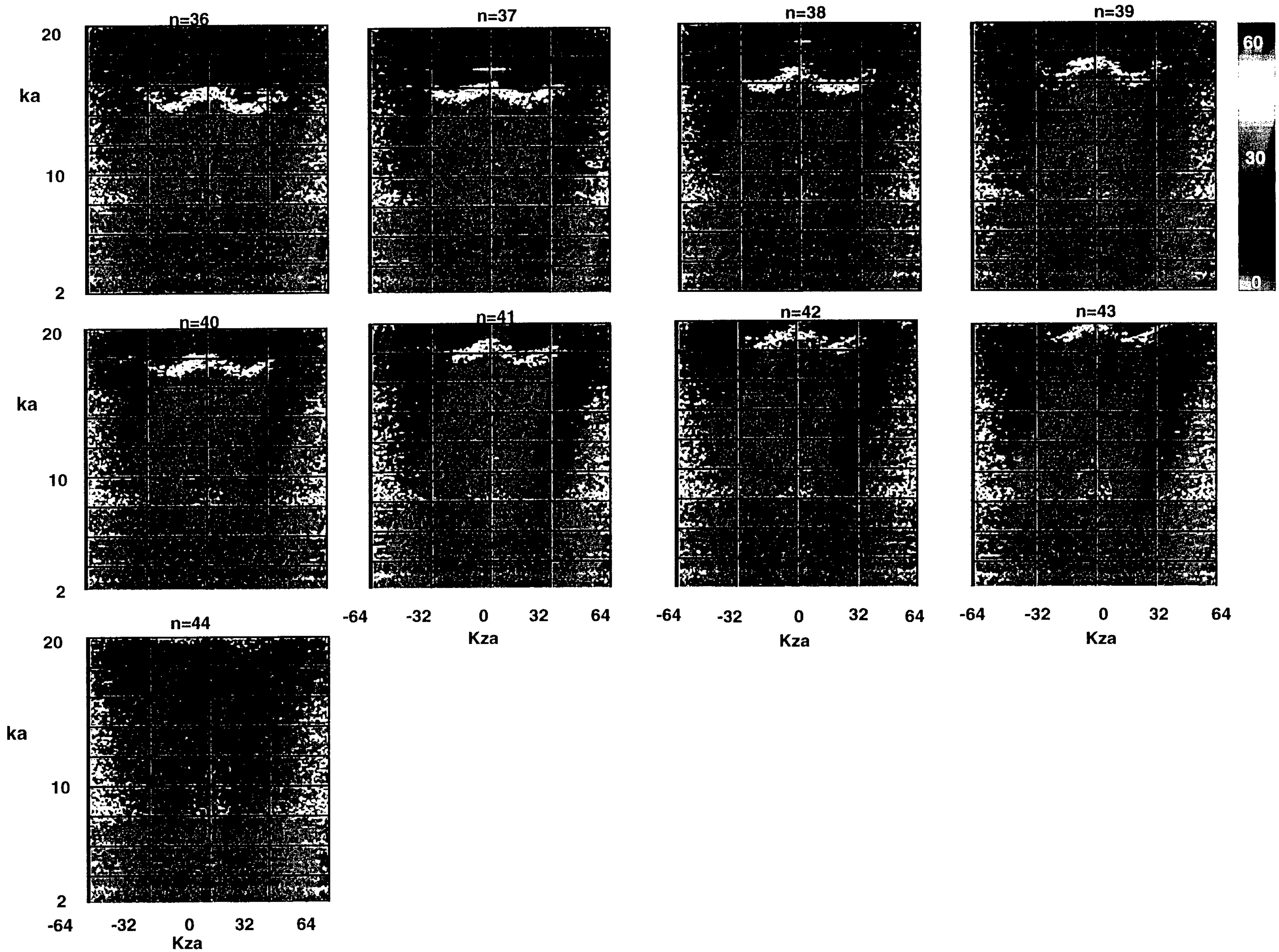

FIG. 25. Reconstructed pressure dispersion for 1/50 scale model data (n=36-44), random axial placement error

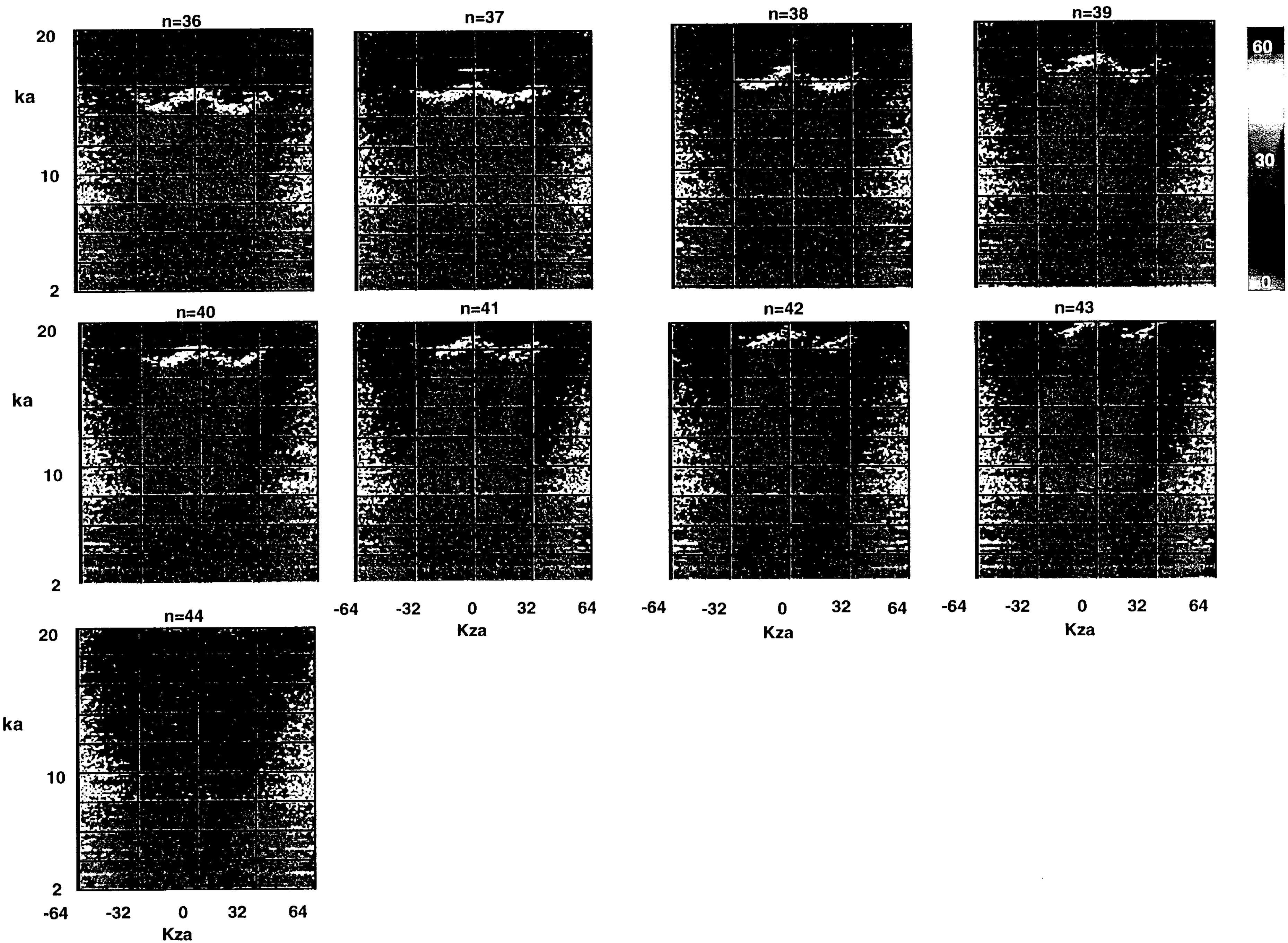

FIG. 26. Reconstructed pressure dispersion for 1/50 scale model data (n=36-44), random circumferential placement error

enough at ISMS to be unaffected by pleasure boating noise. If this turned out to be case, use of NAH would significantly increase the number of hours per day when acoustic measurements could be made.

3. In-plane random errors have the largest contaminating influence on holographic reconstructions, followed by in-plane bias errors. Radial random and bias errors have the smallest contaminating influence.

Future work in the following areas is recommended:

1. Development of improved (and possibly automated) wavenumber filtering techniques.

2. Determine the effect of pleasure boating noise on the ability to implement NAH at ISMS

3. Conduct a study similar to the present one considering the effect of similar contaminating influences on reconstructed velocities, super-sonic and subsonic intensities, and radiated noise.

4. Conduct a parametric study which will generate error curves corresponding to noise and placement contamination of varying magnitudes.

REFERENCES

[1] E.G. Williams and J.D.Maynard, "Holographic imaging without the wavelength resolution limit," Phys. Rev. Let. 45, 554-557 (1980)

[2] J.D. Maynard, E.G. Williams, and Y. Lee, "Near-field acoustical holography (NAH), I. Theory of generalized holography and the development of NAH," J. Acoust . Soc. Am. **78**, 1395-1413 (1985)

[3] E.G. Williams, H.D. Dardy and R.G. Fink, "Near-field acoustical holography using an underwater, automated scanner," J. Acoust. Soc. Am. **78** (2), 789-798 (1985)

[4] E.G. Williams, B.H. Houston and J.A. Bucaro, "Broadband near-field acoustical holography for vibrating cylinders," J. Acoust. Soc. Am. **86** (2), 674-679 (1989

[5] W.A. Veronesi and J.D. Maynard, "Digital holographic reconstructions of sources with arbitrary shaped surfaces," J. Acoust. Soc. Am. **85** (2), 588-598 (1989)

[6] E.G. Williams, H.D. Dardy and R.G. Fink, "A technique for measurement of structureborne intensity in plates," J. Acoust. Soc. Am. **78** (6), 2061-2068 (1985)

[7] E.G. Williams, B.H. Houston and J.A. Bucaro, "Experimental investigation of the wave propagation a point driven, submerged capped cylinder using *K*-space analysis", J. Acoust. Soc. Am. **87** (2), 513-522, (1990)

[8] H. Allik, R. Dees, S.Moore and D. Pan, "SARA-2D User's Manual," Version 95-3, BBN Acoustic Technologies, New London, CT (1995)

[9] W.H. Press, B.P. Flannery, S.A. Teukolsky, and W.T. Vetterling, *NUMERICAL RECIPIES, The Art of Scientific Computing*, Cambridge University Press, 1986

[10] E.G. Williams, "Near-field holographic results for the C-50," NRL Technical Report, In Publication.

[11] T. Luce and S. Hayek, "An examination of filter effects in cylindrical near-field holography," Proceedings of Noise-Con 87, State College, PA (1987)

[12] P.S. Watkinson, "Calibration and inherent errors of a two hydrophone sound intensity measurement system," Proc. Inst. Acoustics, Vol. 6, Pt.5 (1984)

[13] J.A. Clark and D. Feit, "Time varying wave-number frequency spectra" J. Acoust. Soc. Am., Supp (1), **84**, A. (1988)

[14] D. Photiadis, B. Houston, and E.G. Williams, "Wave-number space response of a near-periodically ribbed shell", J. Acoust. Soc. Am., **101** (2), Feb. 1997

Distribution List

CENTER DISTRIBUTION

Copies			Copies	Code	Name
4	ONR		1	0110	J. Corrado
1	334	G. Main	1	7000	P. Covich
1	334	A. Tucker	1	7014	R. Stefanowicz
			1	7016	G. Szilagyi
			1	7051	W. Blake
1	334	R. Vogelsong	1	7052	D. Feit
1	334	V. Simmons	1	7053	Y.N. Liu
			1	7200	J. King
3	NRL		1	7250	P. Shang
1	5136	E Williams	10	7250	G. Carroll
1	5136	B. Houston	1	7250	K. Jones
1	5136	J. Bucaro	1	7250	J. Niemiec
			1	7250	E. O'Neill
			1	7250	S. Fisher
2	NAVSEA		1	7250	D. Warwick
1	92R	G. Jebsen	1	7250	R. Vasudevan
1	03T	R. Taddeo	1	7310	W. Hoover
			1	7310	S. Schreppler
2	DTIC		1	7340	J.A. Clark
			1	7340	D. Groutage